Ethylene and ROS Signaling Are Key Regulators of Lateral Root Development under Salt Stress in Tomato

Maryam Rahmati Ishka[1], Jiantao Zhao[1], Hayley Sussman[1], Devasantosh Mohanty[2], Li'ang Yu[1], Eric Craft[3], Miguel Pineros[3], Mark Tester[4], Dorota Kawa[5], Ron Mittler[2], Andrew Nelson[1], Zhangjun Fei[1], and Magdalena Julkowska[1,4*]

email + ORCID:

Maryam Rahmati Ishka[1] - ORCID - 0000-0002-5447-643X - mri23@cornell.edu

Jiantao Zhao[1] - ORCID - 0000-0002-5140-8220 - jz426@cornell.edu

Hayley Sussman[1] - ORCID - 0000-0002-1331-3319 - hs995@cornell.edu

Devasantosh Mohanty[2] - ORCID 0000-0003-2614-6852 - dm5h8@missouri.edu

Li'ang Yu[1] - ORCID - 0000-0002-9556-011X - ly76@cornell.edu

Eric Craft[3] - ORCID - 0000-0003-0966-8296 - ejc35@cornell.edu

Miguel Pineros[3] ORCID - 0000-0002-7166-1848 - map25@cornell.edu

Mark Tester[4] - ORCID - 0000-0002-5085-8801 - mark.tester@kaust.edu.sa

Dorota Kawa[5] - ORCID - 0000-0002-4227-1621 - d.kawa@uu.nl

Ron Mittler[2] - 0000-0003-3192-7450 - mittlerr@missouri.edu

Andrew Nelson[1] - ORCID - 0000-0001-9896-1739 - an425@cornell.edu

Zhangjun Fei[1] - ORCID - 0000-0001-9684-1450 - zf25@cornell.edu

Magdalena M. Julkowska[1,4] - ORCID - 0000-0002-4259-8296

* correspondence - mmj55@cornell.edu

Affiliations:

1 - Boyce Thompson Institute, Ithaca, NY, USA

2 - Division of Plant Science and Technology, College of Agriculture Food and Natural Resources, Christopher S. Bond Life Sciences Center, 1201 Rollins St., University of Missouri, Columbia, MO 65211, USA.

3 - USDA-ARS, Ithaca, NY, USA

4 - Center for Desert Agriculture, King Abdullah University of Science and Technology, Thuwal, Saudi Arabia

5 – Environmental and Computational Plant Development & Plant Stress Resilience, Utrecht University, Utrecht, The Netherlands

Abstract

Roots are the primary site for sensing salt, making them critical to understanding how plants adapt to salinity. Unraveling the genetic and molecular mechanisms that maintain root growth under salt stress is essential for developing resilient crops. Tomatoes are vulnerable to salinity, as over 50% of arable land is projected to become saline by 2050. While salt stress effects on tomato seed germination, shoot growth, and fruit yield are well-documented, the genetic basis of root development under salinity remains underexplored. Previous studies focused on physiological responses of roots in a narrow range of cultivated-tomatoes, overlooking the genetic diversity for salt resilience in wild-relatives like *Solanum pimpinellifolium*. Here, we investigated salt-induced changes in root system architecture (RSA) across a natural diversity panel of 220 wild- and 25 cultivated-tomato varieties. We identified tolerant accessions with different RSA strategies; prioritizing lateral root elongation versus emergence. To identify genes involved in specific aspects of lateral root development, an F1 hybrid was generated that exhibited both parents' combined characteristics. An F2-segregating population was then used to identify four distinct subpopulations for Bulk Segregant Analysis (BSA). Simultaneously, we conducted Genome-Wide-Association Studies (GWAS) on root architecture of wild-tomato accessions under salt stress. By integrating the results of BSA and GWAS, we identified 22 candidates involved in the maintenance of root architecture. We utilized RNA-Seq to examine transcriptome reprogramming of the 22 genes in tomato accessions with contrasting lateral root responses. This approach resulted in the identification of 2 genes, AP2-like-ethylene-responsive transcription factor TOE3 and L-ascorbate peroxidase. Using exogenous ethylene, we demonstrated that root architecture exhibits plasticity, which benefits the plant by reducing Na^+ accumulation. We profiled H_2O_2 waves across root systems of tomatoes, emphasizing the role of ROS in maintaining root system architecture under salt stress. These findings provide novel genetic targets for enhancing salt resilience in tomatoes, opening avenues for future research and breeding programs.

Introduction

Tomatoes are one of the most widely cultivated and economically significant crops globally, contributing substantially to food security and agricultural economies. With projections indicating that over 50% of arable land will become saline by 2050, understanding tomato responses to diverse saline environments becomes paramount (Roșca et al. 2023). In arid regions, where evaporation rates exceed freshwater input, soil salinization is contentiously increasing (Richards 1969; Abrol et al. 1988; Fischer et al. 2021). These dryland areas, including regions in South America, Southern and Western Australia, Mexico, Southwest United States, and South Africa, have been identified as hotspots for soil salinization (Hassani et al. 2021). Additionally, salt interactions with clay particles result in impenetrable claypan that prevents roots from reaching deeper soil levels (Cione et al. 2000).

Roots are the primary site of salinity sensing and serve to integrate salt stress with other environmental factors, such as nutrient and water availability. The susceptibility of roots to salt stress determines the plant's overall productivity (Atkin et al. 1973; Steppuhn and Raney 2005). Therefore, understanding the molecular processes leading to maintained root growth is necessary for enhancing crop environmental resilience. Although the effects of salt stress on tomato plants have been studied in the context of seed germination, shoot growth, and fruit yield (Manaa et al. 2011; Yang et al. 2019; Sousa et al. 2022; Morton et al. 2023), the impact of salt stress on root architecture remains unexplored. Furthermore, previous studies have primarily focused on a limited number of cultivars and assessed physiological responses (Manaa et al. 2011), rather than elucidating the genetic basis of salt resilience. As freshwater scarcity intensifies, unraveling root-driven salt stress resilience is key to boosting global agricultural productivity and sustainability (Asins et al. 2010; Melino and Tester 2023).

Wild relatives of crops possess valuable traits such as disease resistance, stress tolerance, and nutritional quality, which can be introduced into cultivated varieties through breeding programs (Dempewolf et al. 2014; Ebert and Schafleitner 2015; Brozynska et al. 2016; Pailles et al. 2020; Li et al. 2023). Understanding the genetic basis of these traits in wild relatives facilitates the development of more resilient crop varieties, which are crucial for ensuring food security in the face of environmental challenges. The closest wild relative of cultivated tomato, *Solanum pimpinellifollium* (Pease et al. 2016), shows high tolerance to many biotic and abiotic stresses (Yassin 1985; Sarfatti et al. 1991; Paran and van der Knaap 2007; Ashrafi et al. 2009; Celik et al. 2017; Zhang et al. 2018). However, only a few studies explored the genetics underlying salinity tolerance within *S. pimpinellifolium* natural diversity panels (Rao et al. 2015; Wang et al. 2020b; Morton et al. 2023).

Here, we investigated salt-induced changes in root architecture across a natural diversity panel of 220 wild- and 25 cultivated-tomato varieties. We conducted Genome-Wide-Association Studies (GWAS) on root architecture of wild-tomato accessions under salt stress and identified 55 putative candidate loci. We identified tolerant accessions with different lateral root characteristics, prioritizing either lateral root elongation or emergence. By crossing the tolerant accessions, we generated F1 hybrids that exhibited both parents' combined characteristics. We developed an F2-segregating population and identified four distinct subpopulations for Bulk Segregant Analysis (BSA). By integrating the results of BSA and GWAS, we identified 22 candidate genes involved in the maintenance of root architecture. We utilized RNA-Seq to examine transcriptome reprogramming of the 22 genes in tomato accessions with contrasting lateral root responses. This approach enabled identification of four candidate genes, two with existing annotation including AP2-like-ethylene-responsive transcription factor TOE3 and L-ascorbate peroxidase. Using exogenous ethylene, we demonstrated that root architecture exhibits plasticity, which benefits the plant by reducing Na^+ accumulation. We profiled H_2O_2 accumulation across root systems of tomatoes under salt stress, revealed a unique ROS accumulation pattern associated with maintaining root system architecture of different accessions under salt stress. These findings provide novel genetic targets for enhancing salt resilience in tomatoes, opening avenues for future research and breeding programs.

Results

Wild tomato shows high variation in lateral root development in response to salt stress.

Using an agar plate system, we evaluated 220 *S. pimpinellifolium* accessions for their responses to salt stress (**Table S1**). The 4-day-old seedlings were transferred to media containing 0 or 100 mM NaCl and scanned daily. Although the images were collected for one week after transfer, the root architecture was quantified exclusively for the first 4 days after transfer due to root architecture complexity in a plate setup. We have calculated the daily Main Root growth rate (**Fig. 1A, Fig. S1**), increase in Lateral Root number (**Fig. 1B**), and increase in average Lateral Root Length (**Fig. 1C**) using linear functions. Although salt treatment only slightly decreased the Main Root Growth Rate from 1.334 to 1.275 cm / day (**Fig. 1A**), there was a significant effect of both treatment (ANOVA p-value of 0.000157) and genotype (ANOVA p-value < 2-e16), and interaction between genotype (G) x treatment (T) (**Fig. 1D**, ANOVA *GxT* p-value of 9.56e-16). On the other hand, Lateral Root emergence was substantially decreased by salt stress (from 4.482 to 2.219 LR / day). This interaction was significantly affected by genotype (**Fig. 1 E**, ANOVA *GxT* p-value of 3.59e-14). Similar to the Main Root growth rate, the Lateral Root growth rate showed little decrease in response to salt stress (from 0.315 to 0.304 cm / day), and this phenotype was exclusively affected by genotype (ANOVA p-value < 2e-16), but not by environment (ANOVA p-value of 0.188) or interaction between genotype and environment (**Fig. 1F**, ANOVA *GxT* p-value of 0.383). To evaluate the extent to which root architecture is reprogrammed in response to salt stress, meaning whether individual root architecture components are affected differently, we calculated stress tolerance indices (STI = GR at 100 mM / GR at 0 mM NaCl, **Fig. 1G**). We observed significant differences between individual root

architecture components, with the increase in lateral root number being affected the most (0.494 of the control values) and average lateral root growth being affected the least (1.034 of the control value). Additionally, we observed a significant interaction between the root architecture component and the genotype (Kruskal-Wallis p-value < 2.2e-16), indicating that the tomato root architecture is substantially reprogrammed in response to salt stress. Within the root architecture patterns in the entire diversity panel, we observed that the genotypes that tend to maintain a high number of lateral root numbers, tend to be compromised in their lateral root elongation, while the genotypes that tend to maintain a high lateral root elongation are oftentimes compromised in their lateral root emergence (**Fig. 1G**). These results suggest that the natural variation in *S. pimpinellifolium*'s root architecture in response to salt stress is primarily caused by its differential sensitivity to salt stress in lateral root development.

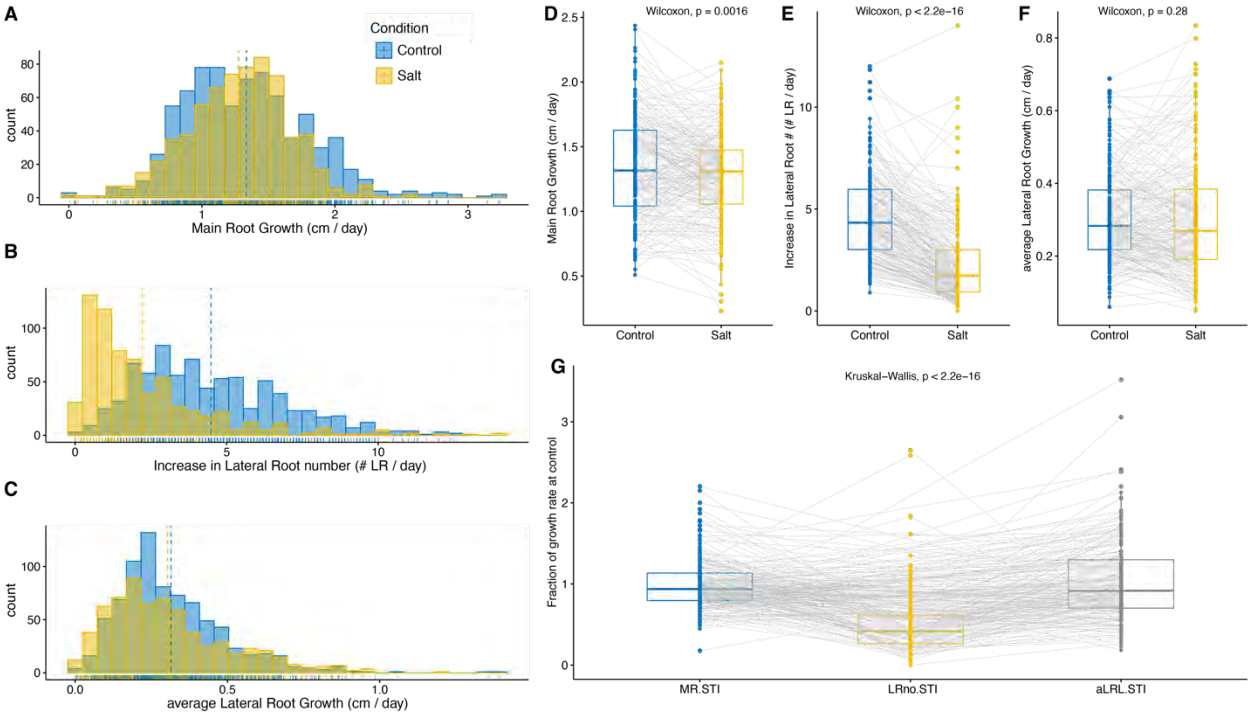

Figure 1. Diversity of salt stress responses observed within the S. pimpinellifolium diversity panel. The 220 genotypes of S. pimpinellifolium were germinated on ½ MS agar plates for 4 days and subsequently transferred to media containing 0 or 100 mM NaCl (Control and Salt respectively). The seedlings were imaged every 24 h after transfer for 7 consecutive days. The Root Architecture of seedlings was quantified for the first 4 days after transfer, and the **(A)** growth of Main Root, **(B)** increase in Lateral Root number and **(C)** growth of average Lateral Root was estimated using linear growth functions. The population average values for Control and Salt conditions are indicated using the dashed lines. The effect of the treatment was evaluated using a paired Wilcoxon test for **(D)** Main Root Growth Rate, **(E)** increase in Lateral Root number and **(F)** average Lateral Root Growth Rate. The individual gray lines illustrate the genotype-specific change in individual growth parameters across the conditions. **(G)** The genotype-specific growth rates at individual conditions were used to calculate the Stress Tolerance Index (STI) for individual traits, calculated by dividing growth rate estimated under Control / Salt conditions. The relative change in STI represents the salt-induced reprogramming of the root architecture. The individual gray lines represent the genotype-specific change in STI across individual components of root architecture. The individual dots represent the genotype-specific mean calculated from 4 biological replicates.

Identification of associations with tomato root architecture through GWAS.

To identify genetic components underlying the root system architecture responses to salt stress, the collected phenotypic data were combined with previously developed genotypic data (Morton et al. 2023) and used in Genome Wide Association Study (GWAS). Initially, we removed heterozygous markers, imputed the missing markers, and performed GWAS using ASReml script, similarly to the method described in (Awlia et al. 2021). This method yielded a total of 109 associated SNPs above Bonferroni threshold (LOD > 7.15), with 85 unique SNPs, grouping into 16 individual loci out of which 5 loci were

144 associated exclusively with root architecture measured under salt stress (**Table S2**). However, this method
145 required us to use a heavily reduced set of SNPs (708 545). Therefore, we explored additional associations
146 using an entire set of 17 962 579 SNP using the EMMAX model with corrections for population structure
147 (using three PCA) and kinship matrix (Kang et al. 2010). Although no overlap was found between ASReml
148 and EMMA-X based scripts, we identified additional 82 associations above the Bonferroni threshold (>
149 8.56) with various root system architecture components (**Table S2**). Only one of the significantly
150 associated SNPs had a minor allele frequency (MAF) > 1% (chromosome 1, position 1369582), associated
151 with lateral root distribution over the length of main root (calculated as Center of Gravity) for roots grown
152 under control conditions (**Table S2**). We further inspected associations with LOD score above 5,
153 considering MAF, and the number of SNPs within the 10 kbp interval to select associations that can be
154 pursued further. We identified 55 genetic loci, each containing at least 3 SNPs within 10 kbp interval or
155 mapped/associated with multiple root architecture traits (**Table S2**). Additionally, we adjusted the
156 Bonferroni threshold to 6.77 as the number of SNPs with MAF > 5% was reduced to 5 944 147.
157 The highest-ranking loci for biomass distribution between main and lateral roots in the first two
158 days (MRLpTRS) were identified on chromosomes 3 and 4, with one locus on chromosome 3 (29 SNPs)
159 and three on chromosome 4 (240, 39, and 85 SNPs) (**Fig. S2A-B**). The chromosome 3 locus mapped to
160 Spimp03g102810, encoding an ABC transporter A family member 7 (**Fig. S2C**). On chromosome 4, the loci
161 spanned a region containing multiple functionally diverse genes, including DUF4283 proteins, L-ascorbate
162 oxidases, MADS-box proteins, RING domain-containing proteins, and a Zinc knuckle CCHC-type family
163 protein (**Fig. S2D-F**). For lateral root length and number after one day of salt stress, high-ranking loci were
164 found on chromosomes 1, 3, and 11 (**Fig. S3A-B**). On chromosome 1, 27 SNPs were located in the promoter
165 region of Spimp01g004220, encoding a LITAF domain-containing protein (**Fig. S3C**). Three SNPs on
166 chromosome 3 spanned genes involved in glycosylation, protein transport, and tRNA synthesis (**Fig. S3D**).
167 The chromosome 11 locus (60 SNPs) was mapped to Spimp11g311320, encoding a chloroplast ribosome-
168 recycling factor, alongside neighboring genes with roles in storage and redox regulation (**Fig. S3E**).
169 Additional loci were linked to increased lateral root number and main root elongation under salt stress
170 (**Fig. S4A-B**). On chromosome 12, 16 SNPs were associated with Spimp12g340040, encoding a glucan
171 endo-1,3-beta-D-glucosidase (**Fig. S4C**). Another 15 SNPs on chromosome 11 were mapped to genes
172 encoding two unknown proteins and a dephospho-CoA kinase (**Fig. S4D**). Other loci with more than 10
173 highly associated SNPs were identified on chromosomes 1, 2, 5, and 12, linked to root traits under control
174 and salt stress conditions (**Fig. S5A-I**).

175 **LA2540 and LA1511 prioritize different aspects of lateral root development under salt stress.**
176 Based on the root system architecture responses to salt stress observed in the diversity panel, we selected
177 two accessions for further detailed investigation. We selected LA2540 as wild tolerant (referred hereafter
178 as wild tolerant) accession, and LA1371 as wild sensitive (referred hereafter as wild sensitive) accession.
179 Additionally, we included an *S. lycopersicum* accession (LA1511, referred hereafter as cultivated tomato),
180 based on the root system architecture responses to salt stress observed in the cultivated diversity panel
181 and its overall similarity in plant morphology to *S. pimpinellifolium* observed in the greenhouse conditions
182 (e.g. plant and fruit size). Salt stress reduced main root growth (**Fig. 2A**), lateral root length (**Fig. 2B**), and
183 the number of lateral roots (**Fig. 2C**) across all examined accessions. While the STI of the main root did not
184 differ across examined genotypes (**Fig. 2D**), substantial differences were observed between wild-tolerant
185 and cultivated tomatoes in lateral root-related traits (**Fig. 2E-F**). Wild-tolerant accession showed a higher
186 STI for average lateral root elongation (**Fig. 2E**), whereas cultivated tomatoes exhibited a higher STI for
187 lateral root emergence (**Fig. 2F**). Additionally, we evaluated the selected genotypes for ion accumulation
188 using ICP-AES after 10 days of exposure to salt stress (**Fig. 2G and Fig. S6**). Salt stress exposure resulted in
189 increased and decreased Na^+ and K^+ accumulation respectively, with no significant differences between

the genotypes. Although all accessions maintained a similar Na^+/K^+ ratio in the roots, cultivated tomatoes exhibited a significantly lower Na^+/K^+ ratio in the shoot compared to both wild accessions. In summary, we have identified LA1511 as a salt-tolerant *S. lycopersicum* line that prioritizes the development of new lateral roots, while LA2540 as a tolerant *S. pimpinellifolium* line that prioritizes the elongation of existing lateral roots.

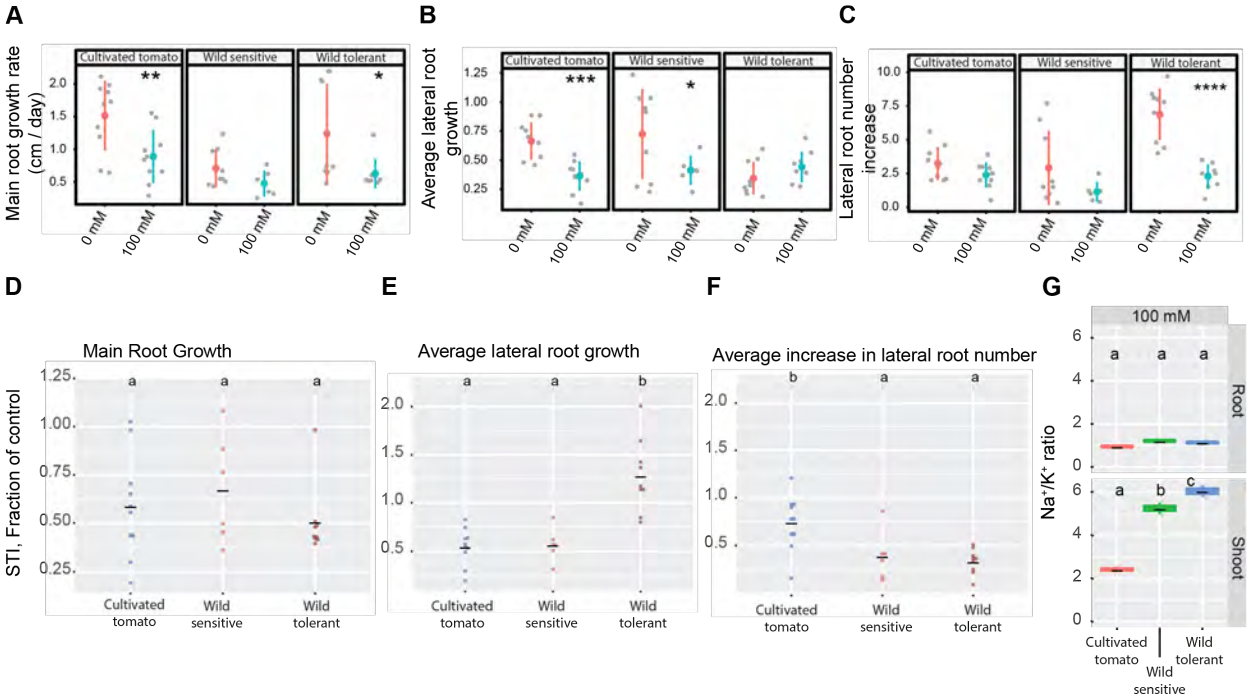

Figure 2. Wild tolerant and cultivated tomatoes have different salt tolerant features regarding lateral root development under the salt. (A-C) Root system architecture analysis of cultivated and wild tomatoes under 0 or 100 mM concentrations of NaCl are shown. **(D)** Salt tolerance indexes (STIs) are shown for the main root, **(E)** average lateral root length, **(F)** and lateral root number. The STI was calculated by dividing the growth rate measured under salt stress by the growth rate measured under control condition for each accession. **(G)** Na+/K+ ratio in root and shoot of different accessions after 10 days on treatment plates. Each dot represents an individual replicate per accession. Lines in (A-C) graphs represent median values. The asterisks above the graphs in (A-C) indicate significant differences between control and salt stress conditions, as determined by the Student 's t-test: *P < 0.05, **P < 0.01, ***P < 0.001, and ****P < 0.0001. Statistical analysis was done by comparison of the means for all pairs using Tukey HSD test for (D-G). Levels not connected by the same letter are significantly different (P < 0.05).

Compound effect of F1 hybrid on maintenance of lateral root development under salt stress.

To further evaluate the genetic mechanisms underlying the differential responses of lateral roots between wild tolerant and cultivated tomato and explore whether the salt tolerance mechanisms are complementary between these two accessions, we generated an F1 hybrid by crossing cultivated and wild-tolerant tomato accessions (**Fig. 3**). We investigated root system architecture of F1 individuals along with their parental lines and wild sensitive accession, under non-stress and salt stress conditions (**Fig. 3 and Fig. S7**). While no significant differences were observed in the main root growth rate between the examined accessions under control conditions (**Fig. 3B**), F1 displayed a significant increase in main root growth rate under the salt stress compared to the other three genotypes, especially when compared to both wild tomatoes (**Fig. 3B**). F1 and cultivated tomatoes showed an increase in lateral root growth rate compared to two wild tomatoes under control conditions (**Fig. 3C**). Under salt stress, F1 individuals exhibited a remarkable increase in lateral root growth rate compared to all other accessions (**Fig. 3C**). Regarding increase in lateral root number, F1 and wild-tolerant accession exhibited higher rate of lateral

root emergence compared to cultivated and wild-sensitive accessions under control condition (**Fig. 3D**), while no significant differences were observed for absolute emergence rates under salt stress (**Fig. 3D**).

To investigate how salt stress impacted various aspects of root architecture, we calculated the STI for main root growth, lateral root elongation, and increased lateral root number (**Fig. 3E-G**). F1 showed the highest STI for main root and lateral root growth rates, compared to its parental lines, indicating a synergistic interaction on these phenotypes. On the other hand, F1 inherited the STI for lateral root emergence, similar to wild tomatoes. We further evaluated F1 along with their parental lines for Na^+ and K^+ accumulation and observed that F1 seedlings maintained a low Na^+/K^+ ratio in the root and shoot, similar to the cultivated tomato (**Fig. 3H, Fig. S7**). Together, these results indicate that the salt tolerance traits, including maintenance of lateral root development and sodium exclusion, are dominant traits inherited from the tolerant parent. Additionally, F1 displays synergistic effect (hybrid vigor) for main and lateral root growth rates.

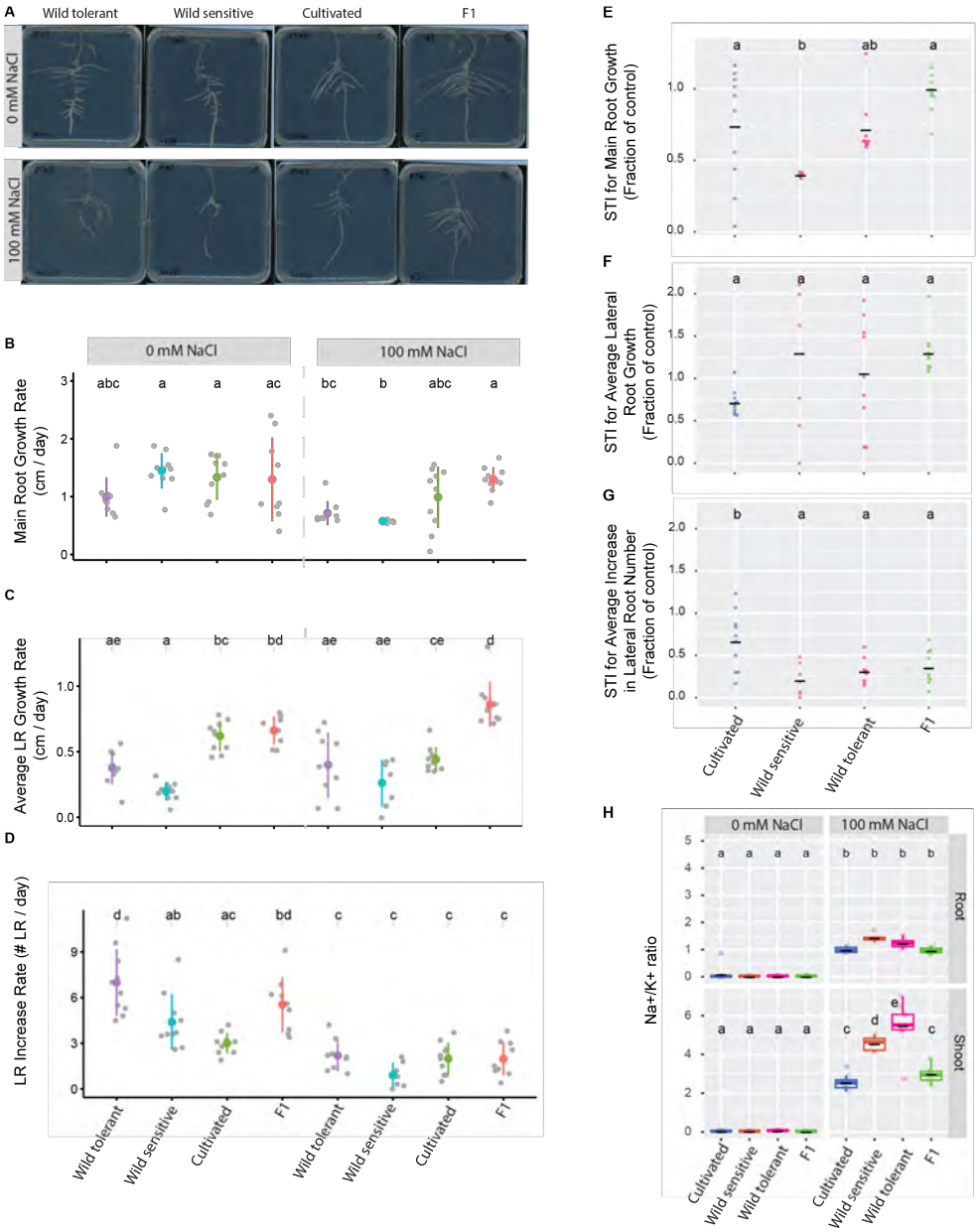

Figure 3. F1 individuals display an increase in main root growth under salt while maintaining lower Na^+/K^+ ratio in root and shoot. Root system architecture of F1 individuals, their corresponding parents, i.e., cultivated and wild tolerant tomatoes along with wild sensitive tomatoes were investigated with and without 100 mM NaCl. **(A)** Shown are representative images of 9-day-old seedlings that experienced 5 days of salt treatment. Growth rate for **(B)** main root length, **(C)** lateral root length, **(D)** and lateral root number. Salt tolerance indexes (STIs) are shown for the **(E)** main root, **(F)** average lateral root length, and **(G)** lateral root number. The STI was calculated by dividing the growth rate measured under salt stress by the growth rate measured under control condition for each accession. **(H)** Na^+/K^+ ratio of root and shoot of different accessions after 10 days on treatment plates. Each dot represents individual replicas per accession. Statistical analysis was done by comparison of the means for all pairs using Tukey HSD test in all graphs. Levels not connected by the same letter are significantly different ($P < 0.05$).

Segregating F2 population reveals loci on chromosomes 3, 6 and 9 to be associated with lateral root development.

To identify genomic regions associated with root system architectural traits under salt stress, we generated the F2 population. We investigated the root system architecture of 180 F2 individuals alongside their parental lines under salt stress and identified four phenotypic sub-populations that segregated into four classes regarding their lateral root phenotypes (**Fig. 4A**). The classes comprised individuals with low lateral root length/low lateral root number (low LRL/low LR.no), high lateral root length/low lateral root number (high LRL/low LR.no), low lateral root length/high lateral root number (low LRL/high LR.no), and high lateral root length/ high lateral root number (high LRL/high LR.no). We pooled 25 seedlings from each sub-population, extracted DNA, and performed whole-genome sequencing in the pools and their two parents for Bulk Segregant Analysis (BSA).

We performed multiple bulk comparisons to identify genomic regions showing the most variation (**Fig. 4B and Fig. S8**). We found significant associations on chromosomes 3 and 6 with lateral root elongation (high LR.no/low LRL vs. low LR.no/high LRL, **Fig. 4B**) and chromosome 9 with lateral root emergence (low LR.no/high LRL vs. high LR.no/high LRL, **Fig. 4B**). Similarly, we observed a region towards the end of chromosome 9 and chromosome 3, associated with overall lateral root development under salt stress (high LR.no/low LRL vs. high LR.no/high LRL, **Fig. 4B**). These results suggest that the genes positioned on chromosomes 3, 6 and 9 are contributing to the differences in lateral root development between wild tolerant and cultivated tomato.

To narrow down the selection of candidate genes within the identified genetic regions, we overlaid the results from BSA and GWAS. We identified nine overlapping loci, and 22 gene coding regions that are putatively associated with lateral root development under salt stress (**Table 1, Table S3**). The candidate genes included: two ABC transporter family member genes (*Spim03g102820* and *Spim05g145990*), associated with the maintenance of main root length and total root system (MRLpTRS.D1&D2. SALT and TRS.D4.SALT.01); two N-acetylglucosaminyltransferase family genes (*Spim03g108680* and *Spim05g145980*) associated with the average lateral root length and total root system (aLRL.D1.SALT and TRS.D4.SALT); transcription factor bHLH87-like (*Spim03g110510*) and AP2-like ethylene-responsive transcription factor TOE3 (*Spim09g252830*), associated with the maintenance of average lateral root length and main root length per total root system (aLRL.D1.SALT and MRLpTRS.D3&D4.SALT). Additionally, we identified genes involved in the regulation of cellular processes such as those encoding a mannan synthase (*Spim09g253730*), a carboxypeptidase (*Spim09g253210*), a subtilisin-like protease (*Spim06g186120*), and a 3'-5' exonuclease domain-containing protein (*Spim03g110520*), associated with maintenance of main root length and average lateral root length per total root system (MRLpTRS.D4.SALT, aLRLpTRS.D2.SALT, and aLRL.D1.SALT). The L-ascorbate peroxidase gene (*Spim09g252840*) was associated with maintaining the main root length per total root system (MRLpTRS.D3&D4.SALT). Additionally, we identified genes encoding two kinases and three proteins of unknown function, including one containing a domain of unknown function (DUF1677, *Spim06g186130*), which were associated with maintaining either lateral root or main root length per total root system (aLRLpTRS.D2.SALT). Although variation within the natural diversity panel is not guaranteed to be captured within bulk-segregant analysis due to differences in allele frequencies and causal genes, we identified overlapping genetic elements contributing to root development under salt stress between GWAS and bulk-segregant analysis.

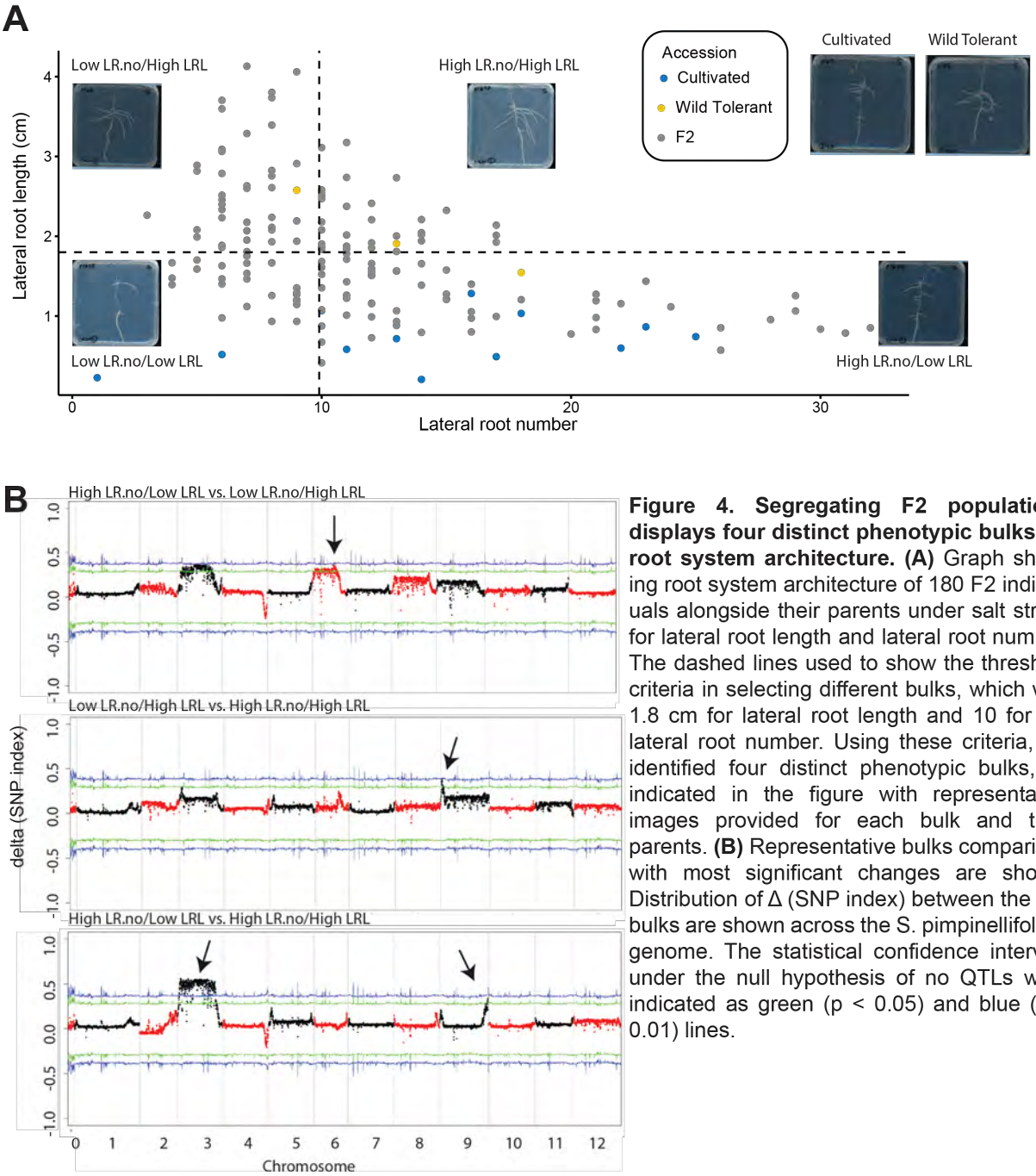

Figure 4. Segregating F2 populations displays four distinct phenotypic bulks for root system architecture. (A) Graph showing root system architecture of 180 F2 individuals alongside their parents under salt stress for lateral root length and lateral root number. The dashed lines used to show the threshold criteria in selecting different bulks, which was 1.8 cm for lateral root length and 10 for the lateral root number. Using these criteria, we identified four distinct phenotypic bulks, as indicated in the figure with representative images provided for each bulk and their parents. **(B)** Representative bulks comparison with most significant changes are shown. Distribution of Δ (SNP index) between the two bulks are shown across the S. pimpinellifolium genome. The statistical confidence intervals under the null hypothesis of no QTLs were indicated as green ($p < 0.05$) and blue ($p < 0.01$) lines.

Identification of transcriptional patterns underlying differences in lateral root development under salt stress.

To identify key time points at which wild tolerant and cultivated tomatoes differ in their lateral root development in response to salt stress, we imaged the development of their root architecture under control and salt stress conditions at 60-minute intervals using a SPIRO setup (Ohlsson et al. 2021)(**Fig. S9**). We observed that salt stress exposure immediately reduces lateral root length in cultivated tomatoes, while no significant differences in individual lateral root length were observed in wild tolerant (**Fig. S9A**). Significant decrease in individual lateral root growth rate was observed from 1,200 minutes after stress

313 exposure onwards in cultivated tomatoes (**Fig. S9B**). On the other hand, there was no obvious difference
314 in lateral root growth rate of wild tolerant until 5,000 minutes after stress exposure, after which salt
315 exposed lateral roots showed an increased growth rate (**Fig. S9B**). Cultivated tomatoes developed new
316 lateral roots throughout the experiment under both control and salt stress conditions, albeit at a reduced
317 rate, thereby reducing the average emergence time from 3519 to 4488 minutes after stress exposure (**Fig.**
318 **S9C**). Although the average emergence time in wild tolerant showed even smaller difference between
319 control and salt stress conditions (2841 and 3173 minutes after stress exposure respectively), we did
320 observe a clear delay in lateral root emergence of wild tolerant under salt stress compared to the control
321 condition, with no lateral roots emerging until 2,000 minutes after stress exposure (**Fig. S9C**).
322 Guided by the time points at which we observed significant differences in lateral root growth and
323 emergence, we performed RNA-Seq analysis of the transcriptional profiles of both cultivated tomato and
324 wild tolerant roots collected at 500, 1000, 2000, 3000, and 4000 minutes after salt stress exposure (**Fig.**
325 **5, Table S4**). We identified 3,792 differentially expressed genes (DEGs) in wild tolerant (2,261 upregulated
326 and 1,531 downregulated) and 4,032 DEGs in cultivated tomato (2,307 upregulated and 1,725
327 downregulated) (**Fig. 5A**). Among these changes, we found 1,467 genes as being upregulated in both
328 accessions while 1,009 genes downregulated. To identify genotype-specific DEGs at specific time points,
329 we compared DEGs across individual time points (**Fig. 5B**). WT showed highest DEGs at 500 min after salt
330 stress exposure (1,796 genes with fold change ≥ 2-fold and adjusted p-value > 0.05), followed by 4,000
331 min (1,631) (**Table S5**). On the other hand, cultivated tomato showed the highest number of DEGs at 4000
332 min (2,018 genes with fold change ≥ 2-fold and adjusted p-value > 0.05), followed by 500 (1,989). While
333 both accessions showed the most changes in transcript abundances during early and late time exposure
334 to salt stress, both had the least changes at 3,000 min after salt exposure. To compare the overlap
335 between time points, we generated UpSet plots (**Fig. 5C, Fig. S10**). This analysis revealed that most
336 upregulated DEGs in each accession were detected at 4,000 minutes, while most downregulated DEGs
337 occurred at 500 minutes (**Fig. 5C**). Additionally, we observed that the majority of DEGs in each accession
338 are unique to one or two time points, with only a few DEGs commonly expressed across all time points.
339 Using gene ontology (GO) enrichment analysis, we examined at which biological process they were
340 involved in. Most DEGs at 500 minutes after salt exposure were enriched with genes involved in stress
341 responses and metabolic processes in wild tolerant, or detoxification and transporter activities in
342 cultivated tomato. Interestingly, at 4,000 minutes, the wild tolerant DEGs remained enriched with genes
343 involved in stress responses and metabolic processes, similar to the early response to stress. In contrast,
344 DEGs found in cultivated tomato showed significant enrichment with genes related to light response,
345 regulatory functions in photosynthesis and cellular binding activities (**Fig. 5C, Table S6**).

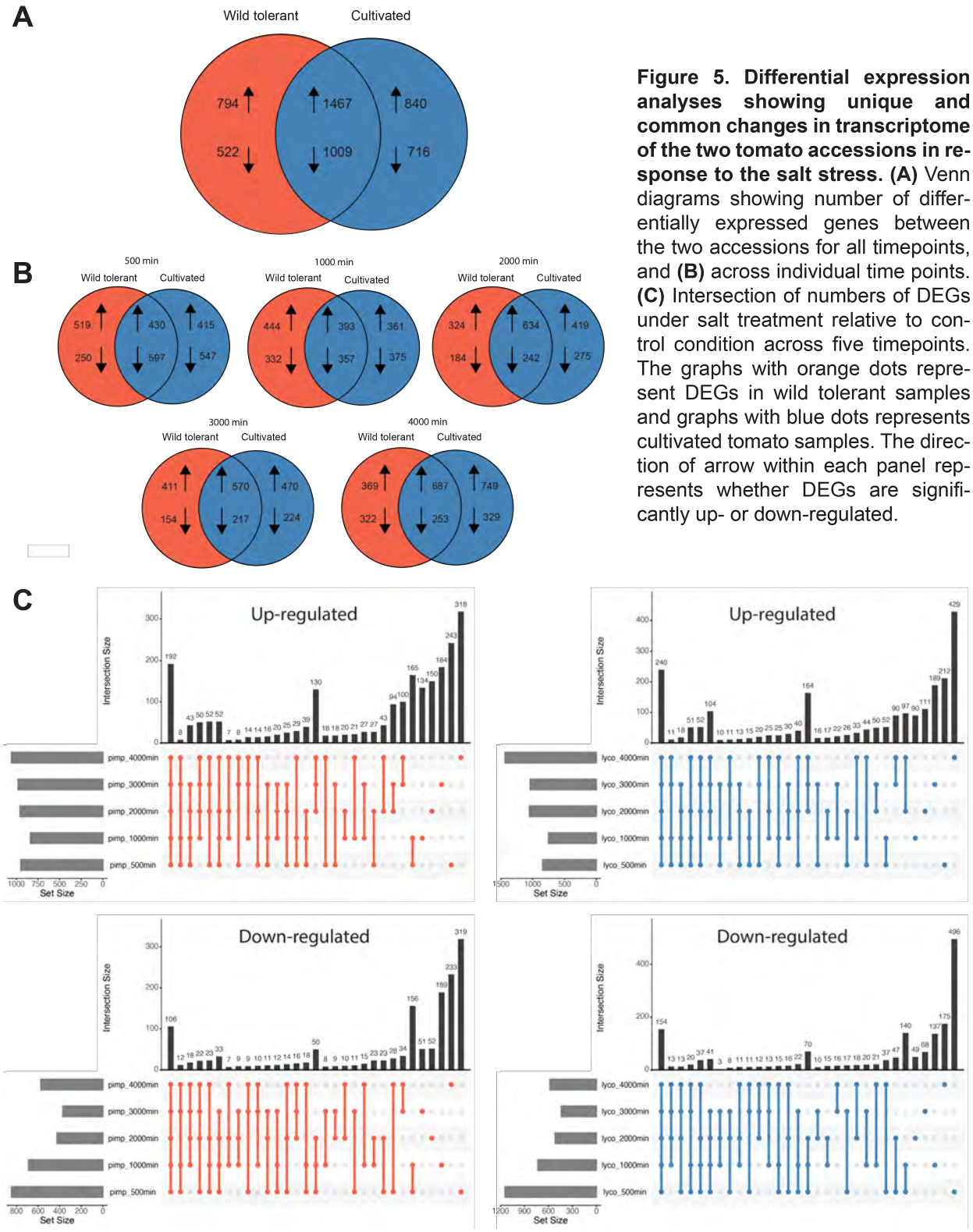

Figure 5. Differential expression analyses showing unique and common changes in transcriptome of the two tomato accessions in response to the salt stress. (A) Venn diagrams showing number of differentially expressed genes between the two accessions for all timepoints, and **(B)** across individual time points. **(C)** Intersection of numbers of DEGs under salt treatment relative to control condition across five timepoints. The graphs with orange dots represent DEGs in wild tolerant samples and graphs with blue dots represents cultivated tomato samples. The direction of arrow within each panel represents whether DEGs are significantly up- or down-regulated.

To uncover transcriptional patterns underlying lateral root differences between accessions, we conducted weighted gene correlation network analysis (WGCNA) (Langfelder and Horvath 2008) and identified 14 co-expression modules (**Fig. 6, Fig. S11**). We focused on modules containing GWAS/BSA candidates and those aligning with contrasting salt stress responses. The **yellow module** (2,697 genes)

exhibited repression from 1,000 min post-stress, more pronounced in cultivated tomato (**Fig. 6A**). It included Spim05g145990, encoding an ABC transporter G family protein, emphasizing the role of cellular transport in root response. The **brown module** (2,907 genes) displayed initial repression in cultivated tomato, recovering over time, while wild tolerant showed a delayed but stronger resurgence (**Fig. 6B**). It contained Spim09g252850, a kinase-like gene linked to lateral root regulation. The **red module** (1,684 genes) showed early induction in cultivated tomato but later repression, while wild tolerant maintained upregulation (**Fig. 6C**). It included AP-3 complex subunit delta (Spim03g108690) and Ring-box protein 1a (Spim06g186110), involved in protein trafficking and interaction (Lee and Hwang 2014), (Abd-Hamid et al. 2020). The **turquoise module** (6,591 genes) was consistently more expressed in cultivated tomatoes, containing ten GWAS/BSA genes associated with protein homeostasis, signaling, and structural integrity (**Fig. 6D**). The **blue module** (3,427 genes) was upregulated in cultivated tomato under salt stress, with a transient upregulation in wild tolerant (**Fig. 6E**). It included genes related to stress response, oxidative protection, and protein modification. The black module (313 genes) was upregulated early in both accessions but showed no later treatment differences (**Fig. 6F**), featuring Spim03g102820, an ABC transporter A family member 7-like gene. These findings highlight that lateral root responses to salt stress depend on early stress-induced genes (e.g., yellow module) and constitutively differentially expressed genes (e.g., turquoise and blue modules).

Identification of candidate genes highly associated with lateral root development under salt stress.
To identify which of the 22 candidate genes (**Table 1**) exhibited transcriptional changes during root development, we cross-referenced them with the RNA-Seq data (**Table S4, Fig. S12**). While all were expressed across various time points, only four showed significant salt stress-induced changes in at least one accession (**Fig. 7A**): DUF1677 (Spim06g186130), AP2-like ethylene-responsive transcription factor TOE3 (Spim09g252830), L-ascorbate peroxidase (Spim09g252840), and an unknown protein (Spim09g253720). DUF1677 and TOE3 were transiently repressed in both cultivated tomato and wild tolerant, indicating their suppression may be critical for salt stress response. L-ascorbate peroxidase was consistently upregulated in cultivated tomato but only transiently in wild tolerant, suggesting its

Table 1. List of 22 genes identified by cross-referencing GWAS and BSA analysis. If no genes were found within the chromosome regions indicated by the GWAS, we extended the search by 10 kb before and after the original SNP locations.

Locus	1st SNP	Last SNP	Gene ID	Chromosome	Start	End	Strand	Description
MRLpTRS.D1&D2.SALT	58311594	58318648	Spim03g102820	Chr03	58317465	58333842	-	ABC transporter A family member 7-like
aLRL.D1.SALT	62872139	62872729	no candidate					
+/-10k	62862139	62882729	Spim03g108680	Chr03	62862616	62865458	-	Core-2/I-branching beta-1,6-N-acetylglucosaminyltransferase family
			Spim03g108690	Chr03	62868995	62871907	-	AP-3 complex subunit delta
			Spim03g108700	Chr03	62873276	62881576	-	Histidine--tRNA ligase
aLRL.D1.SALT	64342558	64343225	no candidate					
+/-10k	64332558	64353225	Spim03g110510	Chr03	64340070	64341212	-	Transcription factor bHLH87-like
			Spim03g110520	Chr03	64348724	64354128	-	3'-5' exonuclease domain-containing protein
TRS.D4.SALT	2853323	2873370	Spim05g145980	Chr05	2855866	2859416	-	Core-2/I-branching beta-1,6-N-acetylglucosaminyltransferase family
			Spim05g145990	Chr05	2864524	2873811	+	ABC transporter G family member protein
aLRLpTRS.D2.SALT	39476715	39476898	no candidate					
+/-10k	39466715	39486898	Spim06g186100	Chr06	39466736	39467116	-	Receptor-type tyrosine-protein like
			Spim06g186110	Chr06	39470274	39473093	+	Ring-box protein 1a
			Spim06g186120	Chr06	39473899	39476229	-	subtilisin-like protease
			Spim06g186130	Chr06	39481301	39481819	-	Protein of unknown function (DUF1677)
MRLpTRS.D3&D4.SALT	893689	899226	no candidate					
-10k/+10k	883689	909226	Spim09g252830	Chr09	885469	888212	+	AP2-like ethylene-responsive transcription factor TOE3
			Spim09g252840	Chr09	893083	897835	+	L-ascorbate peroxidase
			Spim09g252850	Chr09	901262	910459	+	Kinase
MRLpTRS.D3&D4.SALT	1235817	1235817	no candidate					
-10k/+10k			Spim09g253200	Chr09	1239184	1244087	+	DnaJ protein like
			Spim09g253210	Chr09	1244798	1246201	+	Carboxypeptidase
MRLpTRS.D3&D4.SALT	1278892	1308283	Spim09g253260	Chr09	1289015	1294003	+	TIR domain-containing protein
			Spim09g253270	Chr09	1304169	1306382	+	Protein kinase domain-containing protein
MRLpTRS.D4.SALT	1688182	1701564	Spim09g253720	Chr09	1691928	1693028	+	Unknown protein
			Spim09g253730	Chr09	1694719	1698430	-	Mannan synthase
			Spim09g253740	Chr09	1699511	1699663	+	Unknown protein

377 importance in lateral root development. The unknown protein was upregulated early in wild tolerant but
378 not in cultivated tomato, highlighting a genotype-specific expression pattern.
379 To assess allelic variation, we examined SNPs in these four genes using the Integrative Genomics
380 Viewer (IGV) (**Fig. 7B**). SNPs were detected in their 5' UTR, 3' UTR, and intronic regions, suggesting roles
381 in transcriptional regulation and mRNA stability. Two missense SNPs were identified: one in DUF1677
382 (Proline to Leucine) and one in TOE3 (Ala to Val or Leu to Phe), both differing from the reference *S.*
383 *pimpinellifolium* LA2093 genome. Given the overall conservation of coding sequences between
384 accessions, these findings suggest that regulatory variants likely drive differences in gene expression and
385 function.

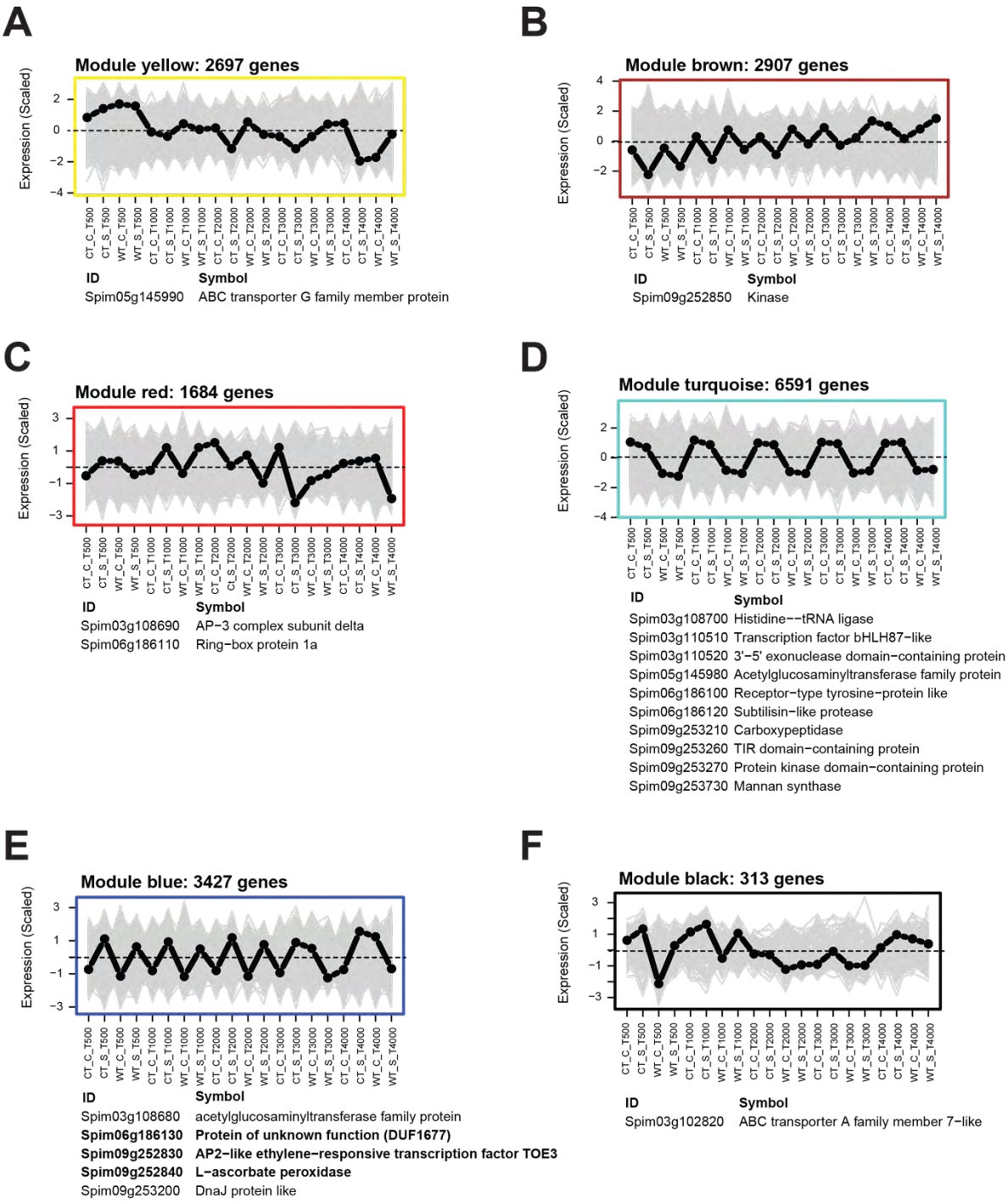

Figure 6. Co-expression network analysis showing distinct patterns among the two accessions across various developmental scales. WGCNA co-expression modules with scaled expression values (y axis) across different time points (x axis) **(A-F)**. Black dotted line indicates eigengene expression profile. Gray line indicates expression values of all genes within the module. Most genes in these modules were positively correlated to the eigengene. Genes that are identified through GWAS and BSA (Table 1) and showing significant association with each module were listed below their respective modules, with bolded genes highlighting three of the four candidates identified by cross-referencing GWAS and BSA with RNA-Seq data. See Fig. S8 for a detailed analysis of all 14 modules.

386

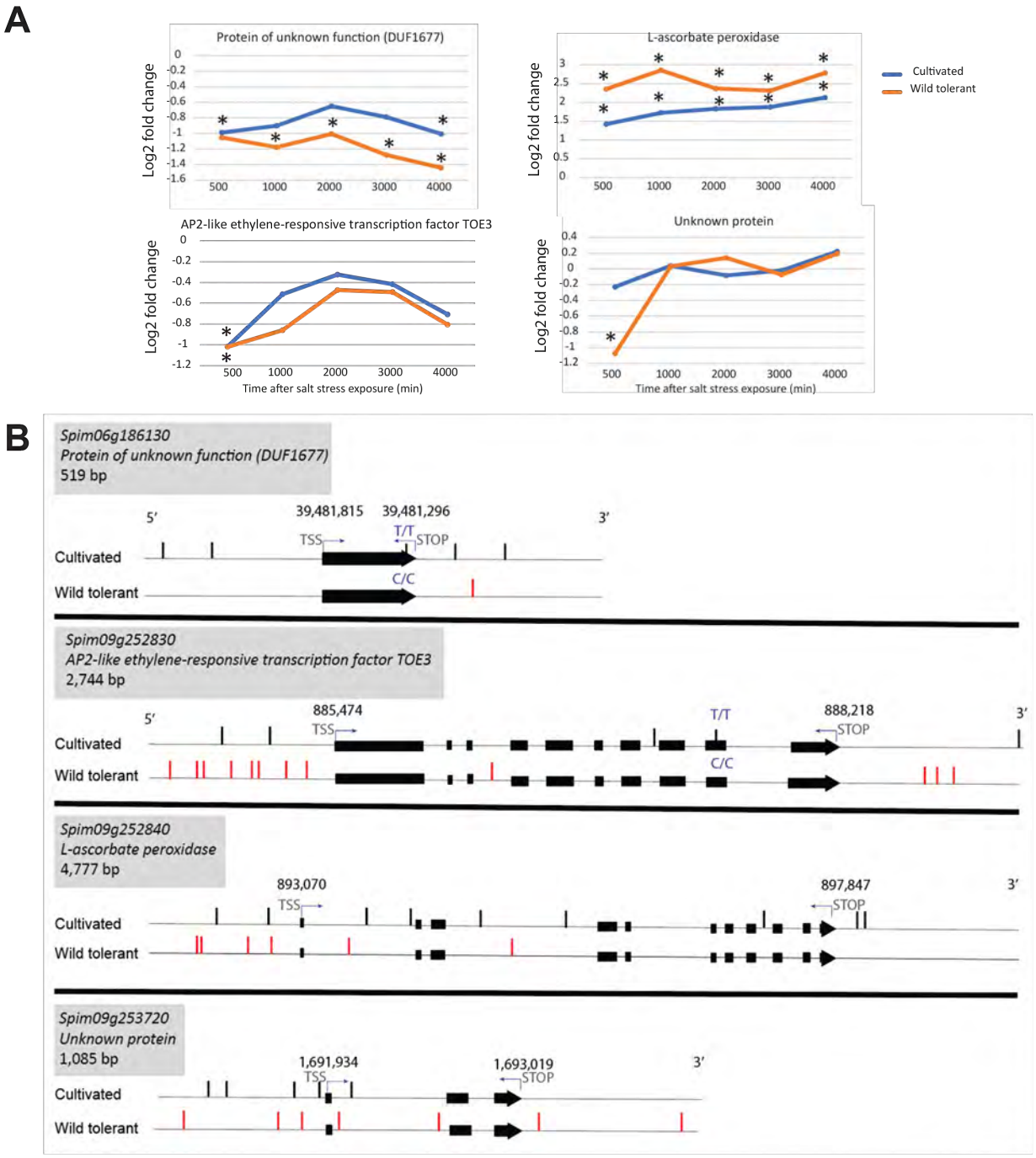

Figure 7. Allelic variants analysis revealed the two accessions are almost conserved in their coding sequence but not in the intronic region, as well as 5' and 3' UTRs. (A) Log2 fold changes are shown for the four genes identified by cross-referencing the three experiments, GWAS, BSA, and RNA-Seq, across all developmental time points for the two accessions. Stars indicate statistically significant changes in gene expression, defined as a fold change of ≥ 2 and an adjusted p-value of < 0.05. **(B)** Gene models are illustrated for the four genes, with unique SNP positions depicted as straight lines. The positions of the transcription start site (TSS) and STOP are indicated, with gene locations displayed above. SNPs resulting in missense mutations are depicted along with their corresponding variants in the other accession. See Table S3 for the comprehensive list of variant analyses conducted for the 22 genes identified from GWAS and BSA analyses (Table 1).

387

ACC reduces root growth without affecting shoot Na^+/K^+ ratio.

Given that TOE3, an AP2-like ethylene-responsive transcription factor, was identified as a key regulator of lateral root development under salt stress (**Fig. 7**), we hypothesized that ethylene is driving the different root architecture strategies in response to salt between cultivated and wild tomatoes. To test this, we analyzed root growth and Na^+ accumulation in two tomato accessions treated with or without the ethylene precursor 1-aminocyclopropane-1-carboxylic acid (ACC). Across all accessions and conditions, ACC significantly reduced both main root and lateral root lengths (**Fig. 8, Fig. S13A-B**), while its effect on lateral root number varied. In cultivated tomatoes, low ACC concentrations significantly reduced lateral root number under both control and salt stress conditions, whereas high concentrations had no effect (**Fig. S13C**). In wild tomatoes, ACC had a non-significant effect under control conditions but significantly increased lateral root number under salt stress at both concentrations. To assess the physiological relevance of these changes, we calculated the STI for root traits (**Fig. 8B-D**). At low ACC concentrations, STI for main root growth significantly decreased in cultivated tomato but remained unchanged at high ACC concentrations (**Fig. 8B**). For lateral root growth, STI increased in cultivated tomato (non-significant at low ACC, significant at high ACC), while in wild tolerant, it significantly decreased (**Fig. 8C**). Lateral root number exhibited a non-significant STI increase in cultivated tomato and no clear trend in wild tolerant (**Fig. 8D**). These findings suggest that ethylene modulates root system architecture in response to salt stress, aligning with transcriptional changes observed in TOE3 (**Fig. 7**). To further explore ACC's role in ion accumulation, we measured Na^+, K^+, and the Na^+/K^+ ratio using ICP-AES. ACC treatment resulted in a non-significant reduction of Na^+ levels in roots and shoots (**Fig. S13D**) and a slight decrease in root K^+ content, while shoot K^+ levels remained unchanged (**Fig. S13E**). In cultivated tomato, the Na^+/K^+ ratio showed no change in roots at low ACC concentration but a non-significant increase at high ACC; in shoots, it decreased slightly at both concentrations (**Fig. 8E**). In wild tolerant, the Na^+/K^+ ratio showed a slight non-significant increase in roots and a mixed response in shoots. These results suggest that ACC-induced root

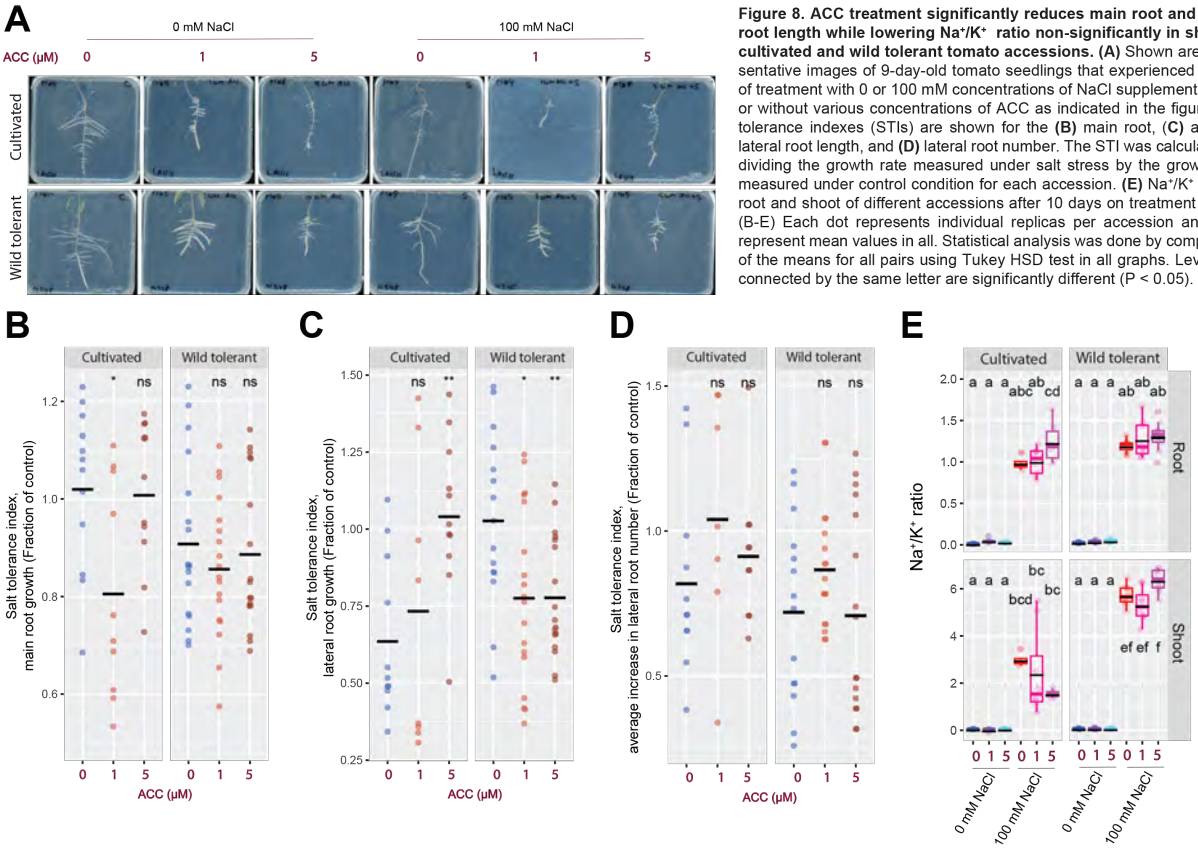

Figure 8. ACC treatment significantly reduces main root and lateral root length while lowering Na^+/K^+ ratio non-significantly in shoot of cultivated and wild tolerant tomato accessions. (A) Shown are representative images of 9-day-old tomato seedlings that experienced 5 days of treatment with 0 or 100 mM concentrations of NaCl supplemented with or without various concentrations of ACC as indicated in the figure. Salt tolerance indexes (STIs) are shown for the **(B)** main root, (**C**) average lateral root length, and **(D)** lateral root number. The STI was calculated by dividing the growth rate measured under salt stress by the growth rate measured under control condition for each accession. **(E)** Na^+/K^+ ratio of root and shoot of different accessions after 10 days on treatment plates. (B-E) Each dot represents individual replicas per accession and lines represent mean values in all. Statistical analysis was done by comparison of the means for all pairs using Tukey HSD test in all graphs. Levels not connected by the same letter are significantly different ($P < 0.05$).

412 architectural changes under salt stress influence Na^+ and K^+ accumulation, potentially contributing to
413 stress resilience.

414 **Ascorbate and H_2O_2 modulate root architecture and K^+ retention under salt stress.**
415 Since APX was identified as a key candidate in lateral root development under salt stress (**Fig. 7**), we
416 hypothesized that ROS homeostasis influences root system architecture under these conditions. To test
417 this hypothesis, we analyzed root traits in two accessions under salt stress, with and without ascorbate
418 (reducing agent) or H_2O_2 (oxidizing agent). Main root length and lateral root growth were largely
419 unaffected by both treatments (**Fig. S14A-B**). However, in cultivated tomatoes, both ascorbate and H_2O_2
420 significantly increased lateral root number under control conditions but had no effect under salt stress,
421 while wild tomatoes showed no significant response across treatments (**Fig. S14C**). Consistent with
422 previous findings (**Fig. 2E-F**), cultivated tomato showed a higher STI for lateral root number, while wild
423 tolerant had a higher STI for lateral root length (**Fig. 9A**, red highlights). Ascorbate had no significant effect
424 on STI for main root length in cultivated tomato but caused a slight, non-significant decrease in wild
425 tolerant (**Fig. 9A**, green font). STI for lateral root traits remained mostly unchanged, except for a slight,
426 non-significant increase in lateral root length in wild tolerant. Similarly, H_2O_2 caused no significant changes
427 in STI values, except for a slight increase in lateral root growth in cultivated tomato and a slight decrease
428 in lateral root number (**Fig. 9A**). These results indicate that exogenous ascorbate and ROS influence root
429 system architecture in a genotype-specific manner.
430 To determine whether ascorbate and H_2O_2 treatments affect ion exclusion and Na^+ and K^+
431 homeostasis, we measured ion content in roots and shoots using ICP-AES (**Fig. S14D-E**). Neither treatment
432 significantly altered Na^+ content in either accession (**Fig. S14D**). Under control conditions, both treatments
433 slightly increased root K^+ content in cultivated tomato, while no significant changes were observed in wild
434 tolerant. Under salt stress, ascorbate caused a slight but non-significant increase in root K^+ content in both
435 accessions, while H_2O_2 had no effect (**Fig. S14E**). In shoots, ascorbate led to a slight, non-significant K^+
436 increase in cultivated tomato, whereas H_2O_2 had no detectable effect. In wild tolerant, ascorbate did not
437 affect shoot K^+ levels under control conditions, but H_2O_2 caused a minor increase. Under salt stress, shoot
438 K^+ content changes mirrored those in cultivated tomato (**Fig. S14E**). Regarding the Na^+/K^+ ratio, neither
439 treatment significantly altered root ion balance, but ascorbate significantly reduced the Na^+/K^+ ratio in
440 shoots under salt stress in both accessions (**Fig. 9B**). These results suggest that ascorbate enhances salt
441 tolerance primarily by maintaining cellular K^+ homeostasis.

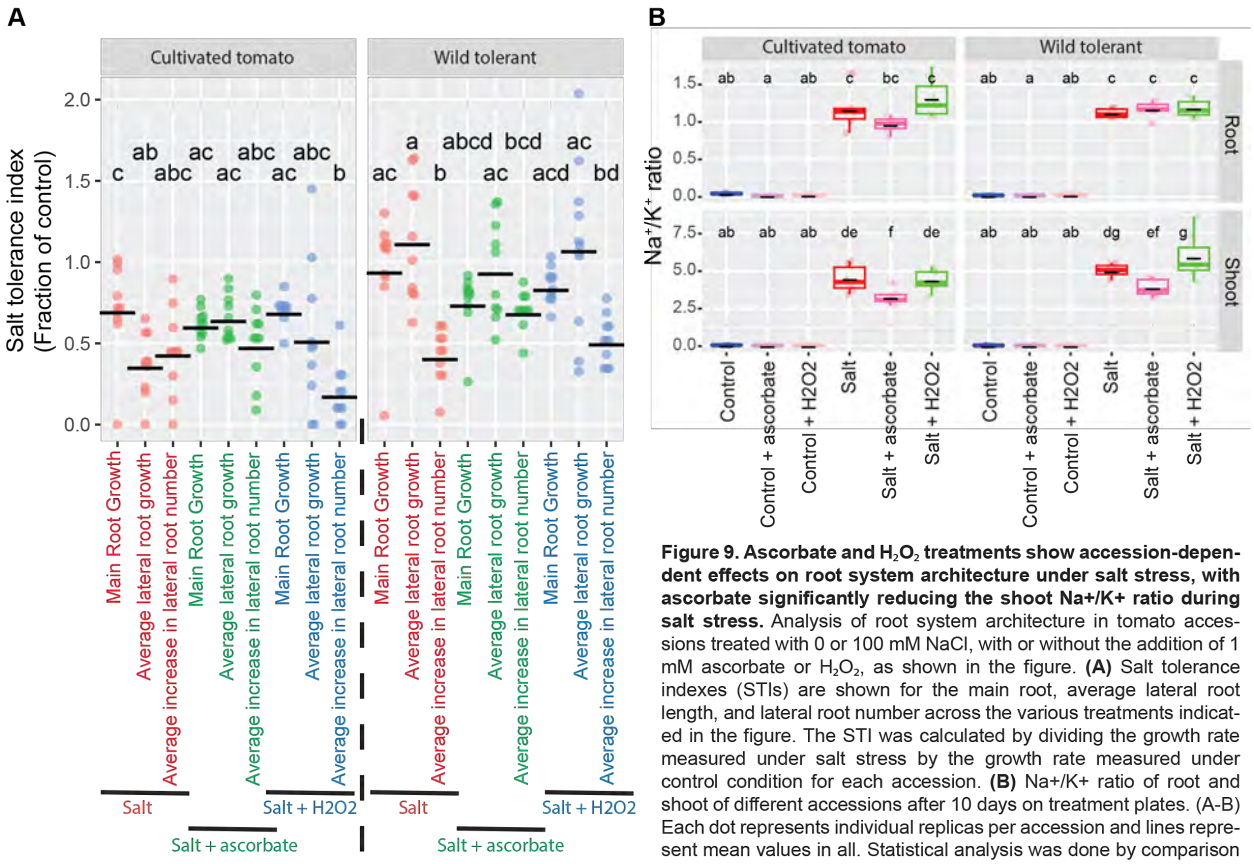

Figure 9. Ascorbate and H_2O_2 treatments show accession-dependent effects on root system architecture under salt stress, with ascorbate significantly reducing the shoot Na+/K+ ratio during salt stress. Analysis of root system architecture in tomato accessions treated with 0 or 100 mM NaCl, with or without the addition of 1 mM ascorbate or H_2O_2, as shown in the figure. **(A)** Salt tolerance indexes (STIs) are shown for the main root, average lateral root length, and lateral root number across the various treatments indicated in the figure. The STI was calculated by dividing the growth rate measured under salt stress by the growth rate measured under control condition for each accession. **(B)** Na+/K+ ratio of root and shoot of different accessions after 10 days on treatment plates. (A-B) Each dot represents individual replicas per accession and lines represent mean values in all. Statistical analysis was done by comparison of the means for all pairs using Tukey HSD test in all graphs. Levels not connected by the same letter are significantly different ($P < 0.05$).

H_2O_2 accumulation under salt stress displays distinct responses among the two accessions.

Given that we identified APX as a key candidate gene involved in lateral root development under salt stress (**Fig. 7**), and observed APX differential transcriptional responses among accessions in the transcriptome profiling, we hypothesized that the two accessions exhibit distinct H_2O_2 accumulation patterns upon salt stress in roots that might explain their distinct root architecture. To test this, we imaged H_2O_2 levels in the roots and shoots of both accessions over a time series under salt stress (**Fig. 10**). This analysis revealed that a spike of ROS accumulation occurs in the roots of the cultivated tomato at 20 and 30 minutes after salt exposure ($p = 0.1$), which then declined compared to corresponding mock treatments at 240 min (**Fig. 10A**). A similar pattern was not observed in the roots of the wild tolerant tomato (**Fig. 10A**). In contrast, the shoots of the cultivated tomato exhibited a peak in accumulation at 20 minutes ($p = 0.1$), while the shoots of the wild tolerant tomato showed a similar peak earlier at 10 minutes ($p = 0.2$), which continued to increase until 30 minutes after salt exposure (**Fig. 10B**). By 240 minutes post-exposure, both accessions displayed baseline levels of H_2O_2 in their shoots (**Fig. 10B**). Overall, these findings suggest that the two accessions exhibit distinct H_2O_2 signaling dynamics in roots in response to salt stress, which may contribute to their differences in root architecture.

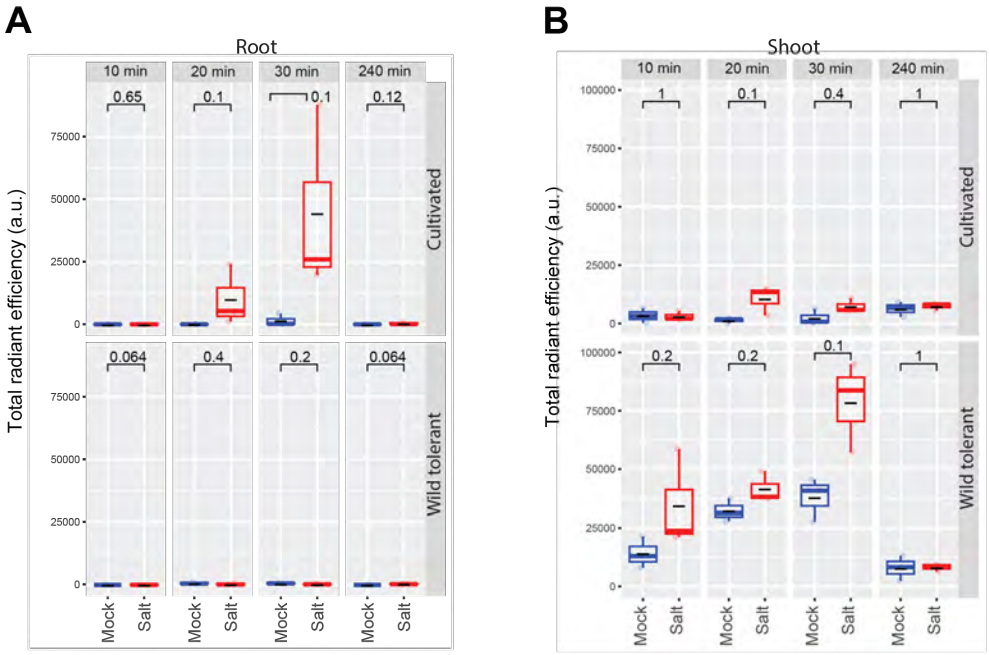

Figure 10. H2O2 profiling in roots shows distinct responses among the two accessions under salt stress. Quantification of H_2O_2 levels in the **(A)** roots and **(B)** shoots of two tomato accessions exposed to 0 or 100 mM NaCl at specific time points, as indicated in the figure. Salt stress was applied by fumigating the plates with a Peroxy Orange 1 (PO1) solution, a H_2O_2-specific dye, containing 100 mM NaCl, while mock-treated plates received only the PO1 solution. Imaging was performed using the IVIS Lumina S5 platform with Living Image 4.7.3 software in acquisition mode. The raw integrated density of regions of interest (ROIs) was quantified using ImageJ. Differences between mock and salt-treated conditions within each accession were analyzed using one-way ANOVA, with n = 3 per accession and condition. a.u. refers to arbitrary units.

Discussion

Harnessing the inherent genetic diversity found in wild relatives, traditional landraces, and modern cultivars is essential for ensuring food security, a critical priority for crop enhancement initiatives. Genetic diversity within the wild progenitors of our cultivated crop species has been largely recognized as an important resource for increasing climate resilience of modern-day agriculture (Kovach and McCouch 2008; Morton et al. 2023). In tomato, GWAS has been used for detecting genetic variations underlying complex agronomic and morphological traits (Bui et al. 2015; Alaguero-Cordovilla et al. 2018; Rodriguez et al. 2020; Tripodi et al. 2021; Ye et al. 2021; Hakla et al. 2024). Although various components of salinity tolerance have been identified in S. pimpinellifolium (Rao et al. 2015; Wang et al. 2020b; Morton et al. 2023), this is the first study that explores root system architecture-derived mechanisms of salt tolerance.

We used a previously developed natural diversity panel of 220 diverse wild tomato accessions to identify alleles associated with root system responses to salt stress. A total of 191 significant associations corresponding to 55 genetic loci have been identified, of which nine showed overlap with BSA and RNA-seq studies. Moreover, we have identified accession LA2540 (wild tolerant) to be salt tolerant, which interestingly was identified as one of the more resilient *S. pimpinellifolium* accessions in field and greenhouse-based studies (Morton et al. 2023). Unlike in Arabidopsis, where natural variation in salt-induced changes in root architecture was observed for both main and lateral root based responses (Julkowska et al. 2017), we have identified that salt-induced changes in *S. pimpinellifolium* root architecture are mainly associated with lateral root development (**Fig. 1, Fig. S2**). We identified a

479 cultivated tomato accession, LA1511, that showed complementary response in its lateral root
480 development to the wild tolerant tomato (**Fig. 2**). Through generation of F1 hybrids between wild tolerant
481 and cultivated tomato, we determined that the lateral root traits of both cultivated and wild tolerant
482 accessions can be combined and act on complementary aspects of salinity tolerance. F1 hybrid exhibited
483 an increase in STI for average lateral root length when compared to each parent (**Fig.3F**). Additionally, F1
484 maintained a lower Na^+/K^+ ratio, mimicking the cultivated parent and prioritizing tolerance by exclusion
485 of sodium in the shoot (Fig. 6H) (Munns and Tester 2008). Together, these findings suggest that combining
486 the complementary strategies of salinity tolerance, based on complementary characteristics of lateral
487 root development, results in increased resilience of F1 hybrids. While previous studies have identified
488 *S.pimpinellifolium* as a resource for salt tolerant traits (Rao et al. 2015; Razali et al. 2018; Martínez-Cuenca
489 et al. 2020), we show that dissecting responses to salt stress through root architecture can result in
490 identification of complementary traits that can be a source of further potentiation of salt stress resilience.
491 BSA identified three genomic regions linked to root growth maintenance under salt stress, and
492 integration with GWAS revealed 22 candidate genes (**Table 1**). While only four showed significant
493 transcript changes (**Fig. 7, Fig. S11**), 17 clustered in WGCNA co-expression modules (**Fig. 6**). Turquoise
494 module contained genes involved in cellular homeostasis, including carboxypeptidase (Spim09g253210)
495 and mannan synthase (Spim09g253730), key players in cell wall remodeling (Website; Voiniciuc 2022;
496 Zhang et al. 2024), subtilisin-like protease (Spim06g186120), thus far mainly studied in the context of
497 plant-pathogen interactions (Figueiredo et al. 2014), and 3'-5' exonuclease domain-containing protein
498 (Spim03g110520), implicated in DNA quality control (Shevelev and Hübscher 2002). Subtilases, known for
499 their glycosylation-dependent activity, are critical for lateral root emergence, as seen in *Arabidopsis*
500 where AIRS subtilase promotes lateral root outgrowth by degrading structural proteins in the extracellular
501 matrix (Neuteboom et al. 1999). While mannan synthase remained repressed under stress, subtilisin-like
502 protease exhibited late-stage upregulation (**Fig. S11**), suggesting distinct regulatory roles in lateral root
503 adaptation to salt stress.
504 AP2-like ethylene-responsive transcription factor TOE3 (Spim09g252830) (**Fig. 6**) showed
505 significant transcript changes under salt stress (**Fig. 7**) and co-localized within chromosome 9 GWAS/BSA
506 regions (**Table 1**). Ethylene-responsive transcription factors regulate stress adaptation, often acting as
507 molecular switches between stress tolerance and growth inhibition (Dubois et al. 2018). Ethylene's role
508 in salt tolerance varies—while enhancing resilience in *Arabidopsis*, it suppresses salt tolerance in *Oryza*
509 *sativa*, where RNAi knockdown of OsEIL1/OsEIL2 improves survival (Cao et al., 2006; Achard et al. 2006;
510 Jiang et al. 2013; Peng et al. 2014). Here, we observed that for both tomato accessions, ACC treatment
511 significantly reduced main and lateral root growth (**Fig. 8, Fig. S13**) but had no significant impact on the
512 shoot Na^+/K^+ ratio, suggesting ethylene limits root exposure to salt rather than directly affecting ion
513 homeostasis. One possible mechanism is the growth restriction hypothesis, where ethylene reduces root
514 surface area, minimizing Na^+ uptake. TOE3 expression was initially repressed in response to salt stress
515 before recovering at later time points (**Fig. 7**), indicating that lateral root development requires dynamic
516 ethylene signaling. The early repression of TOE3 may be essential for lateral root initiation, followed by
517 increased expression during adaptation. This aligns with findings in *Arabidopsis*, where ethylene results in
518 early root growth inhibition through inhibiting cell proliferation and disturbance of microtubules in
519 elongating cells (Street et al. 2015; Wang et al. 2018), but later facilitates root growth through promoting
520 cell elongation via auxin-ethylene-ABA crosstalk (Růzicka et al. 2007; Thole et al. 2014). Together, these
521 results support a model where ROS homeostasis, ethylene signaling, and cell wall remodeling coordinate
522 lateral root development under salt stress. Future studies should explore post-transcriptional regulation
523 of these candidate genes and how ethylene interacts with other hormonal pathways in salt adaptation.
524 Salinity stress leads to oxidative stress and cellular damage. The antioxidant system mitigates
525 oxidative damage by counteracting the generation of reactive oxygen species (ROS) (Wang et al. 2013;
526 Ahanger et al. 2017). Salt tolerance is positively correlated with the cell's antioxidant capacity (Shalata

527 and Neumann 2001; Munns and Tester 2008; Zhang et al. 2012; Wang et al. 2013; Dinneny 2019;
528 Hasanuzzaman et al. 2019; Thabet et al. 2021), additionally supported here by an increase in the
529 expression of ascorbate peroxidase throughout our experiment (**Fig. 7**). The constitutive expression of
530 ascorbate peroxidase can be explained by two potential mechanisms. First, the initial reactive oxygen
531 species (ROS) generated by salt stress trigger root cells to enhance their antioxidant response. Second,
532 the emergence of lateral roots requires cell rupture, which generates another wave of ROS signal in a
533 localized area of the root environment, further amplifying the increase in transcript levels. These potential
534 mechanisms highlight the complex interplay between stress responses and root development. While
535 ascorbate and H_2O_2 treatments showed accession-dependent effects on root system architecture under
536 salt stress, we observed that ascorbate treatment significantly reduced the Na^+/K^+ ratio, primarily by
537 aiding in K^+ retention during salt stress (**Fig. 9, Fig. S14**). Previous studies have demonstrated that the
538 Arabidopsis K^+ efflux channel GATED OUTWARDLY-RECTIFYING K^+ CHANNEL 1 (GORK1, AT5G37500) is
539 activated by hydroxyl radicals (HO•) under salt stress and pathogen attack (Demidchik et al. 2010). Using
540 electron paramagnetic resonance spectroscopy and electrophysiological techniques, it was shown that
541 high NaCl concentrations (100 and 250 mM) stimulate HO• production, activating K^+ channels and causing
542 K^+ efflux from roots. From our root transcriptomics data, we identified three outward-rectifying K^+
543 channels that were differentially expressed in one or both tomato accessions (**Table S7**). Two of these
544 channels (Spim03g099320 and Spim11g313920, both annotated as potassium channel SKOR) were
545 downregulated under salt stress, while the third (Spim05g165150, annotated as potassium channel SKOR-
546 like) was upregulated. Notably, Spim11g313920 shares the highest protein identity with Arabidopsis
547 GORK1 (70%), followed by Spim05g165150 (68%), and Spim03g099320 (59%). Spim11g313920 is
548 downregulated at most time points in our study in both accessions. GORK1 is known to contribute to
549 guard cell membrane potential hyperpolarization by allowing K^+ efflux, a process critical for resetting
550 membrane potential during ion transport cycles. Under salt stress, GORK1 is expected to be upregulated
551 to counterbalance Na^+ influx at the cost of K^+ efflux, maintaining cellular ionic balance. However, in our
552 study, its downregulation suggests an adaptive response to retain K+ in the cytosol, preserving cellular
553 integrity. Since both tomato accessions here demonstrate salt tolerance through distinct lateral root
554 traits, we propose that the addition of ascorbate enhances the downregulation of K^+ efflux channels,
555 supporting K^+ retention in the cytosol. This process helps maintain cellular integrity and promotes lateral
556 root development under salt stress. However, further studies are needed to investigate how ascorbate
557 influences the functionality of K^+ efflux channels beyond changes in gene expression, which is outside the
558 scope of this study. Although both accessions exhibited early H_2O_2 accumulation in shoots in response to
559 salt, the distinct H_2O_2 signaling patterns observed in the roots of the two accessions suggest differential
560 oxidative signaling dynamics that may regulate lateral root development under salt stress. The early and
561 sustained H_2O_2 accumulation in cultivated tomato roots at 20 and 30 minutes (**Fig. 10A**) may contribute
562 to salt-induced lateral root emergence. In contrast, the wild-tolerant accession, which exhibits minimal
563 and delayed H_2O_2 accumulation at 240 minutes, may employ a different strategy to modulate redox
564 signaling, potentially facilitating lateral root elongation. These findings suggest that temporal differences
565 in H_2O_2 accumulation could underlie the contrasting root architectural responses observed between the
566 accessions.

567 In conclusion, our integrative approach successfully identified new and previously known
568 candidate genes involved in lateral root development under salt stress conditions. Our additional
569 physiological experiments provide compelling initial validation that ethylene signaling and the antioxidant
570 scavenging system are pivotal factors in regulating lateral root development under salt stress. Future full
571 genetic validation of the identified genes in both wild and cultivated tomato background will provide more
572 insight into genotype x environment interactions and genetic context of lateral root development.
573 Nevertheless, data generated in this study will prove invaluable for future functional validation studies

aimed at elucidating the precise roles of these genes during early root development in response to salt stress, contributing to the broader objective of enhancing plant productivity under saline conditions.

Materials and Methods

Agar-based plate experiments

Tomato seeds were sterilized for 10 min with 50% bleach and rinsed five times using autoclaved milli-Q water, and germinated on ¼ strength Murashige and Skoog (MS) medium containing 0.5% (w/v) sucrose, 0.1% (w/v) 4-morpholineethanesulfonic acid (MES), and 1% (w/v) agar, with pH adjusted to 5.8 with KOH. After 24 h of vernalization at 4 ˚C in the dark, the plates were placed in the Conviron growth chamber with the light intensity of 130–150 µmol x m^{-2} x s^{-1} in a 20 h light / 4 h dark cycle at 25 ˚C day / 20 ˚C night and 60% humidity. 4 days after germination, the seedlings were transferred to 1/4 MS media with and without 100 mM NaCl, as indicated in the figures. Each plate contained one tomato seedling for root system architecture analysis. The plates were scanned using EPSON scanner every 5 consecutive days, starting from day 4 after germination. To analyze root system architectural traits from the scanned plate images, we used SmartRoot plugin (Lobet et al. 2011) in ImageJ to manually trace the root, and extract root-related features in the CSV format followed by data analysis in R. The root system architecture assays for the initial experiment to evaluate the root system architecture responses of natural diversity panel were conducted over six experimental batches, with four biological replicates per genotype per condition. The quantified data averaged per genotype and condition is listed in Table S1. The original image data, together with the traced files can be found at https://doi.org/10.5061/dryad.nk98sf826. The R-script used to curate and process the raw phenotypic data can be accessed at (https://rpubs.com/mjulkowska/BIGpimp_RSA_salt). The R-notebooks for the analysis of individual follow-up experiments can be accessed at RPubs - 20211201_M248M058LA1511_RSA_analysis, RPubs - 20230502_RSA_F1_100mM_Salt, RPubs - 20230612_F1_FW_DW_ICP_Salt, RPubs - 20230605_RSA_analysis_F2_100mM_Salt_d9_all_batches_final). The data analysis and visualization has been performed using ggplot2, ggpubr, corrplot, ggbeeswarm, ggridges, gapminder, RColorBrewer, ColorRamps, doBy, reshape2, cowplot, plotly and tidyverse libraries (Kassambara; Keitt; Wickham 2016, 2020; Wilke 2016; Wei and Simko 2017; Wickham et al. 2019; Chen 2020; Sievert 2020; Categorical Scatter (Violin Point) Plots [R package ggbeeswarm version 0.7.2] 2023, doBy: Groupwise Statistics, LSmeans, Linear Estimates, Utilities).

Genome wide-association study

The genome wide-association study has been performed using the data from 220 *S. pimpinellifolium* accessions using the ASReml script as described in (Morton et al. 2023). Briefly, the SNP data has been curated and imputed for missing and heterozygous SNPs, and ran using three PCA components as estimations for population structure, and kinship matrix calculated using GAPIT (Wang and Zhang 2021). The code used for running the ASReml-based script can be accessed at https://github.com/mmjulkowska/Pimp_RSA_GWAS_salt/blob/main/20211011_RSA_GWAS_prep.R andhttps://github.com/mmjulkowska/Pimp_RSA_GWAS_salt/blob/main/20220101_ASReml_prep_for_pimp_RSA.R. The ASReml-method GWAS output files can be accessed at https://doi.org/10.5061/dryad.nk98sf826. Additionally, we have used the entire SNP dataset to run EMMA X method (Kang et al. 2010), using 3 PCA components as estimations for population structure, and kinship matrix calculated using the essential SNP set. The code used for running the EMMAX-based script can be accessed at https://github.com/mmjulkowska/Pimp_RSA_GWAS_salt/blob/main/20240208_EMMAX_GWAS%20pip

617 eline.md. The EMMA-X GWAS output files can be accessed at https://doi.org/10.5061/dryad.nk98sf826.
618 The data was subsequently investigated for all SNPs with association p-value above genome-wide
619 threshold of -log10(p-value) > 5, as well as minor allele frequency and overlap of associations across
620 individual traits and neighboring SNPs. The list of strongly associated SNPs can be found in **Table S2**.

621 **Elemental analysis**

622 The elemental analysis was performed using Inductively Coupled Plasma Atomic Emission Spectroscopy
623 (ICP-AES). For analysis of Na^+ and K^+ ions in roots and shoots of plate-grown seedlings, the plants were
624 grown on 1/4 x MS plates as described above. After 10 days of exposure to 0 or 100 mM NaCl, root and
625 shoot tissues were harvested and measured for fresh weight, rinsed in milli-Q water and collected into
626 separate paper bags that were dried at 60 °C for 2-3 days. Subsequently, the dry weight was recorded.
627 Samples were digested in double distilled HNO_3, followed by the addition of 60/40 nitric/perchloric acid
628 (v/v), continuing incubation at 150 °C. Samples were processed for ICP-AES analysis using a Thermo iCap
629 7000 ICP-AES after being diluted to 10 ml with deionized water. Ion content was calculated per dry weight
630 for each sample, followed by data analysis in R.

631 **Generating the F1 hybrid and screening the F2 population for variation in later root length and number**

632 The F1 hybrid population was created through reciprocal crosses between two tomato varieties: the
633 cultivated tomato (*S. lycopersicum* LA1511) and the wild tolerant tomato (*S. pimpinellifolium* LA2540). The
634 F1 hybrid underwent self-pollination to produce the F2 segregating population. From this population, 180
635 F2 tomato seeds were used for Bulk Segregant Analysis (BSA). The seeds underwent processing similar to
636 that described for the agar-based plate experiments mentioned above for screening root system
637 architecture. Following the root system architecture analysis, we identified four distinct bulks within the
638 F2 population based on lateral root length and number. These bulks were then subjected to DNA
639 extraction.

640 **DNA extraction for genome sequencing**

641 From each bulk, we pooled 25 individuals that had the best characteristic of their designated pool for DNA
642 extraction from roots. Extraction of the DNA was carried out using Wizard® Genomic DNA Purification Kit
643 (Promega, catalogue # A1125) according to the manufacturer instructions. The integrity of DNA samples
644 was checked using the electrophoresis gel and the concentration was determined by measuring the
645 absorbance at 260 nm in a Nanodrop. 500 ng/µl of DNA from each pool and the two parents were sent
646 on dry ice to the Novogene (Sacramento, CA, USA) for genome sequencing.

647 **Bulk Segregant Analysis (BSA)**

648 Raw paired-end reads were processed to trim adaptor and low-quality sequences using Trimmomatic
649 (version 0.39) (Bolger et al. 2014). The processed reads were aligned to the reference *Solanum*
650 *pimpinellifolium* genome (Wang et al. 2020a)) using BWA-MEM (0.7.17-r1188) (Li 2013) with default
651 parameters. Following read mapping, duplicated read pairs in each sample were marked using Picard
652 (v2.26.6; http://broadinstitute.github.io/picard/), and SNPs were then called from the marked alignment
653 files using GATK (v4.1.4.1) (McKenna et al. 2010). The called SNPs were filtered using GATK with
654 parameters 'QD < 2.0 || FS > 60.0 || MQ <40.0 || MQRankSum < -12.5 || ReadPosRankSum < -8.0'.
655 For BSA-Seq analysis, in each comparison of two bulks, SNP index of each SNP site was calculated
656 for each bulk by dividing the number of reads harboring the allele of one parent with the total number of
657 reads covering the site. Δ(SNP index) was then calculated by subtracting the SNP index in one bulk from
658 the SNP index in the other bulk. An average Δ(SNP index) in each 200-kb sliding window with a step size
659 of 100 kb across the *S. pimpinellifolium* genome was calculated. The 95% and 99% confidence intervals of
660 the Δ (SNP index) under the null hypothesis of no QTLs were also calculated following the method

661 described in (Takagi et al. 2013). QTLs were then identified as genomic regions with the Δ (SNP index)
662 larger than the threshold ($p < 0.05$).

663 **Root sample collection for RNA-Seq experiment**
664 To determine the time points corresponding to both pre- and post-lateral root emergence in the presence
665 and absence of 100 mM salt, we utilized the Smart Plate Imaging Robot (SPIRO) platform to capture
666 images of tomato seedlings cultivated on agar plates at 30-minute intervals over the course of one week.
667 Subsequently, we analyzed these images using SmartRoot, and processed in an R-pipeline that can be
668 accessed at (https://rpubs.com/mjulkowska/tomato_LR_LA1511vsM248) to identify the time points at
669 which lateral roots emerged. Based on this analysis, we selected five time points spanning before, during,
670 and after lateral root emergence under both control and salt stress conditions, specifically at 500, 1000,
671 2000, 3000, and 4000 minutes after transfer to the treatment plates. Following this selection, we collected
672 root samples, excluding the 0.5 cm root tip, from the two tomato accessions at the designated time points
673 in three independent biological replicates. These samples were promptly frozen in liquid nitrogen and
674 stored at -80°C for subsequent analysis.

675 **RNA isolation, library preparation, and sequencing**
676 Total RNA from roots were extracted using RNeasy Plant Mini Kit (Qiagen, Invitrogen, catalog # 74904),
677 including a cleaning step using RNase-free DNase to eliminate genomic DNA contamination. The integrity
678 and quality of RNA samples were evaluated using the Qubit RNA IQ Assay Kit (ThermoFisher Scientific,
679 catalog # Q33221) and its concentration were evaluated using Qubit RNA HS Assay Kit (ThermoFisher
680 Scientific, catalog # Q32852). 500 ng/µl of total RNA from each sample was sent on dry ice to the
681 Novogene (Sacramento, CA, USA) for library preparation using NEBNext Ultra™ II RNA Kit for Illumina
682 (Catalog# E7770L) paired end x 150 bp unstranded sequencing using NovaSeq. RNA-seq data were
683 processed, in brief, using "trimmomatic" (v0.32, parameter: LEADING:3 TRAILING:3 MINLEN:36, TruSeq3-
684 PE.fa:2:30:10:2, (Bolger et al. 2014)) to remove adaptors and low-quality reads. Then, clean reads derived
685 from *S. pimpinellifolium* and *S. lycopersicum* were mapped to the *S. pimpinellifolium* reference genome
686 by Hisat2 (v2.1.0, parameter: --rna-strandness RF -p 60 --no-softclip, (Kim et al. 2019)). Afterwards, the
687 BAM files were processed by FeatureCounts to quantify transcript abundance at the gene level (v2.0.1
688 (Liao et al. 2014), parameter: -s 1 -p -t mRNA -g ID -O). DESeq2 (v3.19, (Love et al. 2013)) was used to
689 normalize read counts among the 60 samples and identify differentially expressed genes (DEGs). Here, we
690 included the four timepoint (500min, 1000min, 2000min, 3000min, 4000min), two species (*S.*
691 *pimpinellifolium* and *S. lycopersicum*), and treatments (Control and Salt) as the experimental design
692 factors. Then condition-wise DEGs per time points per species were identified using the cutoff of adjusted
693 p-value < 0.05. Intersections of DEGs among time-points and species were characterized by the UpsetR
694 plot function in R (Conway et al. 2017). The effect of timepoints, species, and treatment on transcriptome
695 response was examined by principal component analysis (PCA) using in-house R-scripts
696 (https://github.com/Leon-Yu0320/Tomato-salt-stress-transcriptome). Briefly, the PC values were
697 calculated using the top 25% most variable genes based on standard deviation (SD) the PCA plot was
698 visualized with ggplot2 (Wickham 2016).

699 **Go enrichment analysis**
700 GO term enrichment analysis was performed to identify over-represented GO terms in the biological
701 process category using Blast2GO (v3.1.11) (Conesa and Götz 2008). The Fisher's exact test with the FDR
702 correction for multiple testing was used to determine statistical significance (adjusted P value < 0.05).

703 **Co-expression network analysis**
704 Co-expression network modules were built with the weighted gene correlation network analysis (WGCNA)
705 R package version 1.72-1 (Langfelder and Horvath, 2008). Normalized counts were used as an input and

706 75% of the most variable genes were used for analysis. A scale-free network was created by applying a
707 soft threshold power of 5. We created an unsigned network using the blockwiseModules function with
708 following parameters: corType = bicor, max PO utliers = 0.05, merge Cut Height = 0.4 and max Block Size =
709 25 000. Gene Ontology enrichment analysis was carried out with GoStats R package version 2.62.0 with a
710 standard hypergeometric test, to evaluate the enrichment of categories in each module compared to the
711 set of all genes used to create the co-expression network.

712 **Ethylene, ascorbate, and H_2O_2 treatments for root assay**

713 To analyze root system architecture with ethylene treatment, we utilized the ethylene precursor 1-
714 aminocyclopropane-1-carboxylic acid (ACC). ACC was incorporated into the ¼ MS agar plates at
715 concentrations of 1 µM or 5 µM. After autoclaving the media, ACC was added to the cooled medium after
716 filter sterilization. For ascorbate and H_2O_2 treatments, a concentration of 1 mM was used in the ¼ MS agar
717 plates. To prevent ascorbate degradation, freshly prepared ascorbate solution was sprayed on the
718 seedlings daily throughout the experiment. Similar to ACC, H_2O_2 was added to the cooled ¼ MS medium
719 after filter sterilization.

720 **H_2O_2 imaging**

721 The seeds were germinated for four days on ¼ strength Murashige and Skoog (MS) medium as described
722 in the "Agar-based plate experiments" section above. Salt stress was applied by fumigating the plates with
723 Peroxy Orange 1 (PO1; H_2O_2-specific dye; excitation/emission 540 nm/565 nm; Tocris Bioscience cat-
724 1199576-10-7, Bristol, United Kingdom) solution containing 100 mM NaCl while mock plates were
725 fumigated with only PO1 solution. 10 mL of 100 µM PO1 solutions were made in 10 mM phosphate buffer
726 (pH7.4) containing 0.002% Silwet L-77 (LEHLE seeds, Round Rock, TX, USA). Plates were fumigated with
727 fine mist of dye solutions at designated time points (10, 20, 30, 240 min after salt exposure) in a glass
728 chamber (24.5 x 12.5 x 16.5) as described in (Fichman et al. 2019, 2022; Fichman and Mittler 2020, 2021).
729 The imaging was done using the IVIS Lumina S5 platform via Living Image 4.7.3 software in acquisition
730 mode (PerkinElmer, Waltham, MA, USA) (Fichman et al. 2019; Fichman and Mittler 2020, 2021; Myers et
731 al. 2023) and the raw integrated density of regions of interest (ROIs) was calculated using Image J.

732 Data availability

733 Raw genome sequencing reads from Bulk Segregant Analysis (BSA) and RNA-Seq raw reads have been
734 deposited in the National Center for Biotechnology Information BioProject database under the accession
735 numbers PRJNA1108418 and PRJNA1119579, respectively. The phenotypic data in both raw and
736 processed state, and GWAS results can be accessed at https://doi.org/10.5061/dryad.nk98sf826.

737 Acknowledgments

738 The authors would like to thank BTI and KAUST Greenhouse Teams for caring for the plants. The authors
739 would like to thank Lidor Shaar-Moshe at University of Haifa for their constructive discussions that greatly
740 enriched this work. The authors would like to acknowledge support from the NSF-IOS #2023310 (ADLN)
741 and NSF-IOS #2102120 (ADLN), NSF Mathematical Biology #2244735 (MMJ). The majority of funding for
742 this work was generously provided by KAUST, with baseline funding awarded to Mark Tester and BTI's
743 startup funds awarded to Magdalena Julkowska.

744 Author contributions

745 M.R.I. and M.M.J. conceived the project and wrote the manuscript with inputs from all coauthors, M.M.J.
746 performed GWAS, H.S. and M.M.J quantified the root architecture data for the GWAS population, M.R.I.
747 conducted majority of the experiments including root system architecture analysis of selected accessions,

generation of F1 hybrid and F2 segregating population, root system architecture analysis of F2 population for bulk segregant analysis, collected samples and extracted DNA for bulk segregant analysis, collected samples and analyzed ion content data from ICP-AES, performed root system architecture analysis for ethylene, ascorbate, and H_2O_2 treatments as well as conducted ICP-AES analysis, M.R.I. and M.M.J. both collected samples for the time-series RNA-Seq experiment, M.R.I. extracted RNA for time-series RNA-Seq experiment, E.C. and M.P. helped in ICP-AES, L.Y. and A.D.L.N. performed RNA-Seq DEGs analysis, D.K. performed Co-expression network analysis, J.Z. and Z.F. performed Bulk Segregant analysis and GO enrichment, D.M. and R.M. performed H_2O_2 imaging and data analysis, M.A.T. helped with providing infrastructure for the initial screen and initial funding for the experiments.

Competing interests

The authors declare no competing interests

Correspondence and requests for materials

should be addressed to Dr. Magdalena M. Julkowska (mmj55@cornell.edu).

Figures and tables legend

Table 1. List of 22 genes identified by cross-referencing GWAS and BSA analysis. If no genes were found within the chromosome regions indicated by the GWAS, we extended the search by 10 kb before and after the original SNP locations.

Figure 1. Diversity of salt stress responses observed within the *S. pimpinellifolium* diversity panel. The 220 genotypes of *S. pimpinellifolium* were germinated on ½ MS agar plates for 4 days and subsequently transferred to media containing 0 or 100 mM NaCl (Control and Salt respectively). The seedlings were imaged every 24 h after transfer for 7 consecutive days. The Root Architecture of seedlings was quantified for the first 4 days after transfer, and the **(A)** growth of Main Root, **(B)** increase in Lateral Root number and **(C)** growth of average Lateral Root was estimated using linear growth functions. The population average values for Control and Salt conditions are indicated using the dashed lines. The effect of the treatment was evaluated using a paired Wilcoxon test for **(D)** Main Root Growth Rate, **(E)** increase in Lateral Root number and **(F)** average Lateral Root Growth Rate. The individual gray lines illustrate the genotype-specific change in individual growth parameters across the conditions. **(G)** The genotype-specific growth rates at individual conditions were used to calculate the Stress Tolerance Index (STI) for individual traits, calculated by dividing growth rate estimated under Control / Salt conditions. The relative change in STI represents the salt-induced reprogramming of the root architecture. The individual gray lines represent the genotype-specific change in STI across individual components of root architecture. The individual dots represent the genotype-specific mean calculated from 4 biological replicates.

Figure 2. Wild tolerant and cultivated tomatoes have different salt tolerant features regarding lateral root development under the salt. (A-C) Root system architecture analysis of cultivated and wild tomatoes under 0 or 100 mM concentrations of NaCl are shown**. (D)** Salt tolerance indexes (STIs) are shown for the main root, **(E)** average lateral root length, **(F)** and lateral root number. The STI was calculated by dividing the growth rate measured under salt stress by the growth rate measured under control condition for each accession. **(G)** Na^+/K^+ ratio in root and shoot of different accessions after 10 days on treatment plates. Each dot represents an individual replicate per accession. Lines in (A-C) graphs represent median values. The asterisks above the graphs in (A-C) indicate significant differences between control and salt stress conditions, as determined by the Student 's t-test: *P < 0.05, **P < 0.01, ***P < 0.001, and ****P < 0.0001. Statistical analysis was done by comparison of the means for all pairs using Tukey HSD test for (D-G). Levels not connected by the same letter are significantly different (P < 0.05).

Figure 3. F1 individuals display an increase in main root growth under salt while maintaining lower Na^+/K^+ ratio in root and shoot. Root system architecture of F1 individuals, their corresponding parents, i.e., cultivated and wild tolerant tomatoes along with wild sensitive tomatoes were investigated with and without 100 mM NaCl. **(A)** Shown are representative images of 9-day-old seedlings that experienced 5 days of salt treatment. Growth rate for **(B)** main root length**, (C)** lateral root length, **(D)** and lateral root number**.** Salt tolerance indexes (STIs) are shown for the **(E)** main root, **(F)** average lateral root length**,** and **(G)** lateral root number. The STI was calculated by dividing the growth rate measured under salt stress by the growth rate measured under control condition for each accession. **(H)** Na^+/K^+ ratio of root and shoot of different accessions after 10 days on treatment plates. Each dot represents individual replicas per accession. Statistical analysis was done by comparison of the means for all pairs using Tukey HSD test in all graphs. Levels not connected by the same letter are significantly different (P < 0.05).

Figure 4. Segregating F2 populations displays four distinct phenotypic bulks for root system architecture. (A) Graph showing root system architecture of 180 F2 individuals alongside their parents under salt stress for lateral root length and lateral root number. The dashed lines used to show the

806 threshold criteria in selecting different bulks, which was 1.8 cm for lateral root length and 10 for the lateral
807 root number. Using these criteria, we identified four distinct phenotypic bulks, as indicated in the figure
808 with representative images provided for each bulk and their parents. **(B)** Representative bulks comparison
809 with most significant changes are shown. Distribution of Δ (SNP index) between the two bulks are shown
810 across the *S. pimpinellifolium* genome. The statistical confidence intervals under the null hypothesis of no
811 QTLs were indicated as green ($p < 0.05$) and blue ($p < 0.01$) lines.

812 **Figure 5. Differential expression analyses showing unique and common changes in transcriptome of the**
813 **two tomato accessions in response to the salt stress. (A)** Venn diagrams showing number of differentially
814 expressed genes between the two accessions for all timepoints, and **(B)** across individual time points. **(C)**
815 Intersection of numbers of DEGs under salt treatment relative to control condition across five timepoints.
816 The graphs with orange dots represent DEGs in wild tolerant samples and graphs with blue dots represents
817 cultivated tomato samples. The direction of arrow within each panel represents whether DEGs are
818 significantly up- or down-regulated.

819 **Figure 6. Co-expression network analysis showing distinct patterns among the two accessions across**
820 **various developmental scales.** WGCNA co-expression modules with scaled expression values (y axis)
821 across different time points (x axis) **(A-F).** Black dotted line indicates eigengene expression profile. Gray
822 line indicates expression values of all genes within the module. Most genes in these modules were
823 positively correlated to the eigengene. Genes that are identified through GWAS and BSA (Table 1) and
824 showing significant association with each module were listed below their respective modules, with bolded
825 genes highlighting three of the four candidates identified by cross-referencing GWAS and BSA with RNA-
826 Seq data. See Fig. S8 for a detailed analysis of all 14 modules.

827 **Figure 7. Allelic variants analysis revealed the two accessions are almost conserved in their coding**
828 **sequence but not in the intronic region, as well as 5' and 3' UTRs. (A)** Log2 fold changes are shown for
829 the four genes identified by cross-referencing the three experiments, GWAS, BSA, and RNA-Seq, across all
830 developmental time points for the two accessions. Stars indicate statistically significant changes in gene
831 expression, defined as a fold change of ≥ 2 and an adjusted p-value of < 0.05. **(B)** Gene models are
832 illustrated for the four genes, with unique SNP positions depicted as straight lines. The positions of the
833 transcription start site (TSS) and STOP are indicated, with gene locations displayed above. SNPs resulting
834 in missense mutations are depicted along with their corresponding variants in the other accession. See
835 Table S3 for the comprehensive list of variant analyses conducted for the 22 genes identified from GWAS
836 and BSA analyses (Table 1).

837 **Figure 8. ACC treatment significantly reduces main root and lateral root length while lowering Na^+/K^+**
838 **ratio non-significantly in shoot of cultivated and wild tolerant tomato accessions. (A)** Shown are
839 representative images of 9-day-old tomato seedlings that experienced 5 days of treatment with 0 or 100
840 mM concentrations of NaCl supplemented with or without various concentrations of ACC as indicated in
841 the figure. Salt tolerance indexes (STIs) are shown for the **(B)** main root, **(C)** average lateral root length**,**
842 and **(D)** lateral root number. The STI was calculated by dividing the growth rate measured under salt stress
843 by the growth rate measured under control condition for each accession. **(E)** Na^+/K^+ ratio of root and shoot
844 of different accessions after 10 days on treatment plates. (B-E) Each dot represents individual replicas per
845 accession and lines represent mean values in all. Statistical analysis was done by comparison of the means
846 for all pairs using Tukey HSD test in all graphs. Levels not connected by the same letter are significantly
847 different ($P < 0.05$).

848 **Figure 9. Ascorbate and H_2O_2 treatments show accession-dependent effects on root system architecture**
849 **under salt stress, with ascorbate significantly reducing the shoot Na^+/K^+ ratio during salt stress.** Analysis
850 of root system architecture in tomato accessions treated with 0 or 100 mM NaCl, with or without the

addition of 1 mM ascorbate or H_2O_2, as shown in the figure. **(A)** Salt tolerance indexes (STIs) are shown for the main root, average lateral root length**,** and lateral root number across the various treatments indicated in the figure. The STI was calculated by dividing the growth rate measured under salt stress by the growth rate measured under control condition for each accession. **(B)** Na^+/K^+ ratio of root and shoot of different accessions after 10 days on treatment plates. (A-B) Each dot represents individual replicas per accession and lines represent mean values in all. Statistical analysis was done by comparison of the means for all pairs using Tukey HSD test in all graphs. Levels not connected by the same letter are significantly different ($P < 0.05$).

Figure 10. H_2O_2 profiling in roots shows distinct responses among the two accessions under salt stress. Quantification of H_2O_2 levels in the **(A)** roots and **(B)** shoots of two tomato accessions exposed to 0 or 100 mM NaCl at specific time points, as indicated in the figure. Salt stress was applied by fumigating the plates with a Peroxy Orange 1 (PO1) solution, a H_2O_2-specific dye, containing 100 mM NaCl, while mock-treated plates received only the PO1 solution. Imaging was performed using the IVIS Lumina S5 platform with Living Image 4.7.3 software in acquisition mode. The raw integrated density of regions of interest (ROIs) was quantified using ImageJ. Differences between mock and salt-treated conditions within each accession were analyzed using one-way ANOVA, with n = 3 per accession and condition. a.u. refers to arbitrary units.

Supplemental figures and tables legends

Figure S1. The natural variation in Root System Architecture components in response to salt stress. The 220 genotypes of *S. pimpinellifolium* were germinated on ½ MS agar plates for 4 days and subsequently transferred to media containing 0 or 100 mM NaCl (Control and Salt respectively). The seedlings were imaged every 24 h after transfer for 7 consecutive days. The Root Architecture of seedlings was quantified for the first 4 days after transfer, and inspected for changes throughout time for **(A)** Total Root Size, **(B)** Main Root Length, **(C)** Lateral Root Length, **(D)** Lateral Root Number, **(E)** Center of Gravity (calculated as the position of MR with most Lateral Root Length), and **(F)** ratio of Main Root Length per Total Root Size. The individual lines represent the genotype-specific mean, whereas the dashed lines represent the population average. The *, **, *** and **** represent the significant differences between the treatment at individual time points as tested with two-way ANOVA with p-value < 0.05, 0.01, 0.001 and 0.0001, respectively.

Figure S2. Salt-induced changes in root biomass distribution between main and lateral roots are associated with loci on Chromosomes 3 and 4. Genome Wide Association Study was performed on 9M SNPs using standard EMMA-X method. Only SNPs with minor allele frequency > 0.05 were used for plotting the Manhattan plot for associations identified with **(A)** ratio of main root length to total root size at 1 day and **(B)** two days post transfer to salt stress, with pseudo-heritability values of 0.116 and 0.195 respectively. The red line indicates the Bonferroni threshold, whereas the blue line indicates genome-wide suggestive threshold. **(C)** The significantly associated loci were inspected in further detail for the gene coding sequences within the regions with significantly associated SNPs. The region on chromosome 3 contained 29 SNPs with -log10(p-value) > 5. The three individual loci **(D-F)** identified on chromosome 4 contained 240, 39 and 85 SNPs with -log10(p-value) > 5. The association graph below each locus represents the association strength with the ratio of main root length to total root size at 1 day after salt stress imposition.

Figure S3. Salt-induced changes in lateral root development are associated with loci on chromosomes 1, 3 and 10. Genome Wide Association Study was performed on 9M SNPs using standard EMMA-X method. Only SNPs with minor allele frequency > 0.05 were used for plotting the Manhattan plot for

associations identified with **(A)** average lateral root length and **(B)** lateral root number at one day post transfer to salt stress, with pseudo-heritability values of 0.145 and 0.358 respectively. The red line indicates the Bonferroni threshold, whereas the blue line indicates genome-wide suggestive threshold. **(C)** The significantly associated loci were inspected in further detail for the gene coding sequences within the regions with significantly associated SNPs. The region on chromosome 1 contained 27 SNPs, **(D)** the region on chromosome 3 7 SNPs, and **(E)** region on chromosome 11 contained 60 SNPs with -log10(p-value) > 5. The association graph below each locus represents the association strength with the average lateral root length at 1 day after salt stress imposition.

Figure S4. Emergence of lateral roots and main root growth rate is associated with loci on chromosomes 12 and 22. Genome Wide Association Study was performed on 9M SNPs using standard EMMA-X method. Only SNPs with minor allele frequency > 0.05 were used for plotting the Manhattan plot for associations identified with **(A)** lateral root emergence and **(B)** main root growth rate under salt stress, with pseudo-heritability values of 0.855 and 0.628 respectively. The red line indicates the Bonferroni threshold, whereas the blue line indicates genome-wide suggestive threshold. **(C)** The significantly associated loci were inspected in further detail for the gene coding sequences within the regions with significantly associated SNPs. The region on chromosome 12 contained 16 SNPs, whereas **(D)** the region on chromosome 11 contained 15 SNPs -log10(p-value) > 5. The association graph below each locus represents the association strength with the trait initially associated with that locus.

Figure S5. High-confidence loci identified through GWAS. Genome Wide Association Study was performed on 9M SNPs using the standard EMMA-X method. Only SNPs with minor allele frequency > 0.05 were used for plotting the Manhattan plot for associations identified with **(A)** lateral root number at 2 days after transfer to control conditions. The significantly associated loci on chromosome 5, consisting of **(B)** 15 and **(C)** 11 SNPs were inspected in further detail. **(D)** Associations with the number of lateral roots were identified on chromosome 1, and **(E)** the locus consisting of 14 highly associated SNPs has been inspected in more detail. The red line on Manhattan plots indicates the Bonferroni threshold, whereas the blue line indicates genome-wide suggestive threshold. The association graph below each locus represents the association strength with the trait initially associated with that locus.

Figure S6. Wild tomatoes accumulate higher levels of Na^+ in the shoot compared to cultivated tomato. (A) Na^+ and **(B)** K^+ contents of root and shoot of different accessions after 10 days on treatment plates. Each dot represents an individual replicate per accession. Statistical analysis was done by comparison of the means for all pairs using Tukey HSD test. Levels not connected by the same letter are significantly different ($P < 0.05$).

Figure S7. F1 individuals accumulate less Na^+. (A-C) Root system architecture of F1 individuals, their corresponding parents, i.e., cultivated and wild tolerant tomatoes along with wild sensitive tomatoes were investigated with and without 100 mM NaCl. **(D-E)** Na^+ and K^+ contents of root and shoot of different accessions after 10 days on treatment plates. Each dot represents individual replicas per accession. Statistical analysis was done by comparison of the means for all pairs using Tukey HSD test in all graphs. Levels not connected by the same letter are significantly different ($P < 0.05$).

Figure S8. Remaining bulk comparisons. Displayed here are the additional BSA results that were not shown in Figure 4.

Figure S9. Wild tolerant and cultivated tomatoes show variation in lateral root elongation and emergence under the salt stress. (A) Lateral root length, **(B)** lateral root length growth rate, and **(C)** lateral root number are shown for the two tomato accessions grown in agar plate under 100 mM NaCl. The plates were imaged using SPIRO setup at a 30-min interval for one week. Individual transparent lines indicate

939 the growth trajectory of individual lateral roots, dashed line indicates the growth average per genotype
940 per condition, whereas the shaded area indicates the standard deviation. The differences between
941 Control and Salt conditions were tested within each genotype using one-way ANOVA, with *, ** and ***
942 representing p-values below 0.05, 0.01 and 0.001, respectively. The growth dynamics of lateral roots were
943 measured over two experimental replicates for 4 biological replicates per genotype per condition.

944 **Figure S10. Intersection of DEGs between WT and CT under Salt and Control conditions.** The upset plots
945 highlight the intersection of numbers of DEGs between wild tolerant and cultivated tomato samples
946 across five timepoints under salt and control conditions, respectively. The panel with dark blue dots
947 represents samples under the control condition, while the panel with brown dots are Salt samples. The
948 direction of arrows within each panel indicates whether the depicted genes are up- or down-regulated.

949 **Figure S11. Co-expression network analysis.** The rest of WGCNA co-expression modules are shown here,
950 module 7 to 14.

951 **Figure S12. Gene expression profiles over time for genes identified by overlapping GWAS and BSA**
952 **analyses in Table 1.** Log2 fold changes are shown for the 18 genes identified by cross-referencing the
953 GWAS and BSA, across all developmental time points for the two accessions.

954 **Figure S13. ACC treatment significantly reduces both main root and lateral root lengths while causing a**
955 **non-significant decrease in Na^+ concentrations in the roots and shoots of both accessions under salt**
956 **stress.** Root system architecture analysis of cultivated and wild tomatoes under 0 or 100 mM
957 concentrations of NaCl supplemented with or without various concentrations of ACC, as indicated in the
958 figure, are shown for main root growth rate **(A)**, average lateral root length **(B)** as well as average lateral
959 root number **(C)**. Na^+ **(D)** and K^+ **(E)** content of root and shoot of different accessions after 10 days on
960 treatment plates. (A-E) Each dot represents individual replicate per accession. (D-E) Lines represent mean
961 values. The asterisks above the graphs in (A-C) indicate significant differences between control (i.e., 0 mM
962 NaCl and 0 ACC) and other treatment by the Student 's t-test: *P < 0.05, **P < 0.01, ***P < 0.001, and
963 ****P < 0.0001. Statistical analysis was done by comparison of the means for all pairs using Tukey–Kramer
964 HSD test for (D-E). Levels not connected by the same letter are significantly different (P < 0.05).

965 **Figure S14. Ascorbate and H_2O_2 treatments exhibit accession-dependent effects on root system**
966 **architecture under salt stress, with ascorbate contributing to K^+ retention during salt stress.** Root system
967 architecture analysis of cultivated and wild tomatoes under 0 or 100 mM concentrations of NaCl
968 supplemented with or without ascorbate or H_2O_2, as indicated in the figure, are shown for main root
969 growth rate **(A)**, average lateral root length **(B)** as well as average lateral root number **(C)**. Na^+ **(D)** and K^+
970 **(E)** content of root and shoot of different accessions after 10 days on treatment plates. (A-E) Each dot
971 represents individual replicate per accession. (D-E) Lines represent mean values. Statistical analysis was
972 done by comparison of the means for all pairs using Tukey–Kramer HSD test for (A-E). Levels not
973 connected by the same letter are significantly different (P < 0.05).

974 **Table S1. Root System Architecture traits for *S. pimpinellifolium* diversity panel.** The 89 different
975 phenotypes were recorded for 220 *S. pimpinellifolium* accessions. The traits presented in this table
976 represent the average trait value as calculated based on 4 biological replicates. The trait abbreviations are
977 as follow: aLRL - average Lateral Root Length; aLRLpTRS - ratio of average lateral root length to total root
978 size; CoG - center of gravity calculated as the length of the main root that gives rise to most lateral root
979 biomass; LRL - cumulative lateral root length; LRno - lateral root number, MRL - main root length;
980 MRLpTRS - ratio of main root length to total root size; TRS - total root size. The abbreviations behind the
981 1st dot indicate either the time and treatment at which individual RSA parameters were recorded (0 - 4 -

982 days post treatment application; C and S for Control and Salt stress respectively), or STI - stress tolerance
983 index - calculated by dividing the trait value recorded under Salt stress conditions by value recorded under
984 Control conditions. GR indicates the growth rate, estimated by fitting a linear curve into change of trait
985 over time.

986 **Table S2. GWAS results.** All of the SNPs with -log10(p-value) > 5 ware collated into one table, from two
987 GWAS methods used (ASReml - as used in (Awlia et al. 2021), and EMMA-X). The position of each SNP is
988 indicated in Chr and Pos columns, corresponding to chromosome and position on the chromosome in
989 base pairs as per S.pimpinellifolium genome annotation (Wang et al. 2020a). The distance between
990 neighboring SNPs is indicated in the "dist" column, and distances below 10,000 bp are highlighted in
991 yellow, while distances below 1,000 bp are highlighted in red. The Pval column indicates the P-value
992 associated with each SNP, and MAF indicates the minor allele frequency of that particular SNP. The trait
993 column indicates the specific trait association used, with aLRL representing average lateral root length,
994 MRL main root length, LRL lateral root length, TRS total root size, perc - a percentage of main root length,
995 CoG - center of gravity calculated for lateral root distribution along the main root length, Apical, Branched
996 and Basal indicating the lengths of individual zones as absolute values or (perc) as percentage of the main
997 root length. The traits recorded under Control conditions are colored in blue, while traits recorded under
998 salt stress are colored with pink. The LOD is calculated as -log10(p-value). The Method represents whether
999 an individual association was observed as significant using ASReml or EMMA-X method.

1000 **Table S3. Analysis of allelic variants for the 22 genes that overlap between GWAS and BSA studies.**

1001 **Table S4. RNA-Seq raw reads and differentially expressed genes (DEGs).**

1002 **Table S5. Differentially expressed genes (DEGs) for 500 and 4000 minutes.**

1003 **Table S6. Go enrichment analysis for 500 and 4000 minutes.**

1004 **Table S7. List of potassium channels and transporters with their gene expression profiles in tomato root**
1005 **transcriptomics.**

1006 ## References

1007 **Abd-Hamid N-A, Ahmad-Fauzi M-I, Zainal Z, and Ismail I**. Diverse and dynamic roles of F-box proteins in
1008 plant biology. Planta. 2020:**251**(3):68.

1009 **Abrol IP, Yadav JSP, and Massoud FI**. Salt-affected Soils and Their Management (Food & Agriculture
1010 Org.).

1011 **Achard P, Cheng H, De Grauwe L, Decat J, Schoutteten H, Moritz T, Van Der Straeten D, Peng J, and**
1012 **Harberd NP**. Integration of plant responses to environmentally activated phytohormonal signals.
1013 Science. 2006:**311**(5757):91–94.

1014 **Ahanger MA, Tomar NS, Tittal M, Argal S, and Agarwal RM**. Plant growth under water/salt stress: ROS
1015 production; antioxidants and significance of added potassium under such conditions. Physiol Mol
1016 Biol Plants. 2017:**23**(4):731–744.

1017 **Alaguero-Cordovilla A, Gran-Gómez FJ, Tormos-Moltó S, and Pérez-Pérez JM**. Morphological
1018 Characterization of Root System Architecture in Diverse Tomato Genotypes during Early Growth.
1019 Int J Mol Sci. 2018:**19**(12). https://doi.org/10.3390/ijms19123888

1020 **Ashrafi H, Kinkade M, and Foolad MR**. A new genetic linkage map of tomato based on a Solanum
1021 lycopersicum x S. pimpinellifolium RIL population displaying locations of candidate pathogen
1022 response genes. Genome. 2009:**52**(11):935–956.

1023 **Asins MJ, Bolarín MC, Pérez-Alfocea F, Estañ MT, Martínez-Andújar C, Albacete A, Villalta I, Bernet GP,**
1024 **Dodd IC, and Carbonell EA**. Genetic analysis of physiological components of salt tolerance
1025 conferred by Solanum rootstocks. What is the rootstock doing for the scion? Theor Appl Genet.
1026 2010:**121**(1):105–115.

1027 **Atkin RK, Barton GE, and Robinson DK**. Effect of Root-growing Temperature on Growth Substances in
1028 Xylem Exudate of Zea mays. J Exp Bot. 1973:**24**(2):475–487.

1029 **Awlia M, Alshareef N, Saber N, Korte A, Oakey H, Panzarová K, Trtílek M, Negrão S, Tester M, and**
1030 **Julkowska MM**. Genetic mapping of the early responses to salt stress in Arabidopsis thaliana. Plant
1031 J. 2021:**107**(2):544–563.

1032 **Bolger AM, Lohse M, and Usadel B**. Trimmomatic: a flexible trimmer for Illumina sequence data.
1033 Bioinformatics. 2014:**30**(15):2114–2120.

1034 **Brozynska M, Furtado A, and Henry RJ**. Genomics of crop wild relatives: expanding the gene pool for
1035 crop improvement. Plant Biotechnol J. 2016:**14**(4):1070–1085.

1036 **Bui HH, Serra V, and Pagès L**. Root system development and architecture in various genotypes of the
1037 Solanaceae family. Botany. 2015:**93**(8):465–474.

1038 **Cao WH, Liu J, He XJ, Mu RL, Zhou HL, Chen SY, Zhang JS.** Modulation of Ethylene Responses
1039 Affects Plant Salt-Stress Responses, *Plant Physiology*, Volume 143, Issue 2, February 2007, Pages
1040 707–719, https://doi.org/10.1104/pp.106.094292

1041 **Categorical Scatter (Violin Point) Plots [R package ggbeeswarm version 0.7.2]**. 2023.

1042 **Celik I, Gurbuz N, Uncu AT, Frary A, and Doganlar S**. Genome-wide SNP discovery and QTL mapping for
1043 fruit quality traits in inbred backcross lines (IBLs) of solanum pimpinellifolium using genotyping by
1044 sequencing. BMC Genomics. 2017:**18**(1):1.

1045 **Chen B**. Access Data from the USDA ARMS Data API [R package rarms version 1.0.0]. 2020.

1046 **Cione APP, Schmitt CC, Neumann MG, and Gessner F**. The Effect of Added Salt on the Aggregation of
1047 Clay Particles. J Colloid Interface Sci. 2000:**226**(2):205–209.

1048 **Conesa A and Götz S**. Blast2GO: A comprehensive suite for functional analysis in plant genomics. Int J
1049 Plant Genomics. 2008:**2008**:619832.

1050 **Conway JR, Lex A, and Gehlenborg N**. UpSetR: an R package for the visualization of intersecting sets and
1051 their properties. Bioinformatics. 2017:**33**(18):2938–2940.

1052 **Demidchik V, Cuin TA, Svistunenko D, Smith SJ, Miller AJ, Shabala S, Sokolik A, and Yurin V**.
1053 Arabidopsis root K+ efflux conductance activated by hydroxyl radicals: Single-channel properties,
1054 genetic basis and involvement in stress-induced cell death. J Cell Sci. 2010:**123**:1468–1479.

1055 **Dempewolf H, Eastwood RJ, Guarino L, Khoury CK, Müller JV, and Toll J**. Adapting Agriculture to
1056 Climate Change: A Global Initiative to Collect, Conserve, and Use Crop Wild Relatives. Agroecology
1057 and Sustainable Food Systems. 2014:**38**(4):369–377.

1058 **Dinneny JR**. Developmental Responses to Water and Salinity in Root Systems. Annu Rev Cell Dev Biol.
1059 2019:**35**:239–257.

1060 **doBy: Groupwise Statistics, LSmeans, Linear Estimates, Utilities**. Comprehensive R Archive Network
1061 (CRAN). https://cran.r-project.org/web/packages/doBy/index.html. Retrieved June 5, 2024

1062 **Dubois M, Van den Broeck L, and Inzé D**. The pivotal role of ethylene in plant growth. Trends Plant Sci.
1063 2018:**23**(4):311–323.

1064 **Ebert AW and Schafleitner R**. Utilization of wild relatives in the breeding of tomato and other major
1065 vegetables. . In. Crop Wild Relatives and Climate Change. (John Wiley & Sons, Inc: Hoboken, NJ,
1066 USA), pp. 141–172.

1067 **Fichman Y, Miller G, and Mittler R**. Whole-plant live imaging of reactive oxygen species. Mol Plant.
1068 2019:**12**(9):1203–1210.

1069 **Fichman Y and Mittler R**. Noninvasive live ROS imaging of whole plants grown in soil. Trends Plant Sci.
1070 2020:**25**(10):1052–1053.

1071 **Fichman Y and Mittler R**. Integration of electric, calcium, reactive oxygen species and hydraulic signals
1072 during rapid systemic signaling in plants. Plant J. 2021:**107**(1):7–20.

1073 **Fichman Y, Zandalinas SI, Peck S, Luan S, and Mittler R**. HPCA1 is required for systemic reactive oxygen
1074 species and calcium cell-to-cell signaling and plant acclimation to stress. Plant Cell.
1075 2022:**34**(11):4453–4471.

1076 **Figueiredo A, Monteiro F, and Sebastiana M**. Subtilisin-like proteases in plantâ€“pathogen recognition

1077 and immune priming: a perspective. Front Plant Sci. 2014:**5**:739.

1078 **Fischer, G., Nachtergaele, O. F, Velthuizen V, T. H, Chiozza, F., Franceschini, G., et al.** Global Agro-
1079 Ecological Zones v4 – Model documentation (Food & Agriculture Org.).

1080 **Hakla HR, Sharma S, Urfan M, Mandlik R, Kumawat S, Rajput P, Khajuria B, Chowdhary R, Deshmukh**
1081 **R, Roychowdhury R, et al.** Genome-Wide Association Study (GWAS) for Identifying SNPs and Genes
1082 Related to Phosphate-Induced Phenotypic Traits in Tomato (Solanum lycopersicum L.). Plants.
1083 2024:**13**(3). https://doi.org/10.3390/plants13030457

1084 **Hasanuzzaman M, Bhuyan MHMB, Anee TI, Parvin K, Nahar K, Mahmud JA, and Fujita M**. Regulation of
1085 Ascorbate-Glutathione Pathway in Mitigating Oxidative Damage in Plants under Abiotic Stress.
1086 Antioxidants (Basel). 2019:**8**(9). https://doi.org/10.3390/antiox8090384

1087 **Hassani A, Azapagic A, and Shokri N**. Global predictions of primary soil salinization under changing
1088 climate in the 21st century. Nat Commun. 2021:**12**(1):6663.

1089 **Jiang C, Belfield EJ, Cao Y, Smith JAC, and Harberd NP**. An Arabidopsis soil-salinity-tolerance mutation
1090 confers ethylene-mediated enhancement of sodium/potassium homeostasis. Plant Cell.
1091 2013:**25**(9):3535–3552.

1092 **Julkowska MM, Koevoets IT, Mol S, Hoefsloot H, Feron R, Tester MA, Keurentjes JJB, Korte A, Haring**
1093 **MA, de Boer G-J, et al.** Genetic Components of Root Architecture Remodeling in Response to Salt
1094 Stress. Plant Cell. 2017:**29**(12):3198–3213.

1095 **Kang HM, Sul JH, Service SK, Zaitlen NA, Kong S-Y, Freimer NB, Sabatti C, and Eskin E**. Variance
1096 component model to account for sample structure in genome-wide association studies. Nat Genet.
1097 2010:**42**(4):348–354.

1098 **Kassambara A**. ggpubr:'ggplot2'Based Publication Ready Plots. R package version 0.4. 0.] https://cran-r-
1099 project org/web/packages/ggpubr/indes ….

1100 **Keitt T**. Builds Color Tables [R package colorRamps version 2.3.4]. https://cran.r-
1101 project.org/web/packages/colorRamps/index.html. Retrieved June 5, 2024

1102 **Kim D, Paggi JM, Park C, Bennett C, and Salzberg SL**. Graph-based genome alignment and genotyping
1103 with HISAT2 and HISAT-genotype. Nat Biotechnol. 2019:**37**(8):907–915.

1104 **Kovach MJ and McCouch SR**. Leveraging natural diversity: back through the bottleneck. Curr Opin Plant
1105 Biol. 2008:**11**(2):193–200.

1106 **Langfelder P and Horvath S**. WGCNA: an R package for weighted correlation network analysis. BMC
1107 Bioinformatics. 2008:**9**:559.

1108 **Lee MH and Hwang I**. Adaptor proteins in protein trafficking between endomembrane compartments in
1109 plants. J Plant Biol. 2014:**57**(5):265–273.

1110 **Liao Y, Smyth GK, and Shi W**. featureCounts: an efficient general purpose program for assigning
1111 sequence reads to genomic features. Bioinformatics. 2014:**30**(7):923–930.

1112 **Li H**. Aligning sequence reads, clone sequences and assembly contigs with BWA-MEM. arXiv [q-bioGN].
1113 2013.

1114 **Li N, He Q, Wang J, Wang B, Zhao J, Huang S, Yang T, Tang Y, Yang S, Aisimutuola P, et al.** Super-
1115 pangenome analyses highlight genomic diversity and structural variation across wild and cultivated
1116 tomato species. Nat Genet. 2023:**55**(5):852–860.

1117 **Lobet G, Pagès L, and Draye X**. A novel image-analysis toolbox enabling quantitative analysis of root
1118 system architecture. Plant Physiol. 2011:**157**(1):29–39.

1119 **Love M, Anders S, and Huber W**. Differential analysis of count data – the DESeq2 package. 2013.

1120 **Manaa A, Ben Ahmed H, Valot B, Bouchet J-P, Aschi-Smiti S, Causse M, and Faurobert M**. Salt and
1121 genotype impact on plant physiology and root proteome variations in tomato. J Exp Bot.
1122 2011:**62**(8):2797–2813.

1123 **Martínez-Cuenca M-R, Pereira-Dias L, Soler S, López-Serrano L, Alonso D, Calatayud Á, and Díez MJ**.
1124 Adaptation to Water and Salt Stresses of Solanum pimpinellifolium and Solanum lycopersicum var.
1125 cerasiforme. Agronomy (Basel). 2020:**10**(8):1169.

1126 **McKenna A, Hanna M, Banks E, Sivachenko A, Cibulskis K, Kernytsky A, Garimella K, Altshuler D,**
1127 **Gabriel S, Daly M, et al.** The Genome Analysis Toolkit: a MapReduce framework for analyzing next-
1128 generation DNA sequencing data. Genome Res. 2010:**20**(9):1297–1303.

1129 **Melino V and Tester M**. Salt-Tolerant Crops: Time to Deliver. Annu Rev Plant Biol. 2023:**74**:671–696.

1130 **Morton M, Fiene G, Ahmed HI, Rey E, Abrouk M, Angel Y, Johansen K, Saber NO, Malbeteau Y, Al-**
1131 **Mashharawi S, et al.** Deciphering Salt Stress Responses in Solanum pimpinellifolium through High-
1132 Throughput Phenotyping. bioRxiv. 2023:2023.08.15.553433.
1133 https://doi.org/10.1101/2023.08.15.553433

1134 **Munns R and Tester M**. Mechanisms of salinity tolerance. Annu Rev Plant Biol. 2008:**59**:651–681.

1135 **Myers RJ Jr, Zandalinas SI, and Mittler R**. Live whole-plant detection of rapidly accumulating reactive
1136 Oxygen Species following applied stress in Arabidopsis thaliana. Methods Mol Biol. 2023:**2642**:387–
1137 401.

1138 **Neuteboom LW, Veth-Tello LM, Clijdesdale OR, Hooykaas PJ, and van der Zaal BJ**. A novel subtilisin-like
1139 protease gene from Arabidopsis thaliana is expressed at sites of lateral root emergence. DNA Res.
1140 1999:**6**(1):13–19.

1141 **Ohlsson JA, Leong JX, Elander PH, Dauphinee AN, Ballhaus F, Johansson J, Lommel M, Hofmann G,**
1142 **Betnér S, Sandgren M, et al.** SPIRO – the automated Petri plate imaging platform designed by
1143 biologists, for biologists. bioRxiv. 2021:2021.03.15.435343.
1144 https://doi.org/10.1101/2021.03.15.435343

1145 **Pailles Y, Awlia M, Julkowska M, Passone L, Zemmouri K, Negrão S, Schmöckel SM, and Tester M**.
1146 Diverse Traits Contribute to Salinity Tolerance of Wild Tomato Seedlings from the Galapagos
1147 Islands. Plant Physiol. 2020:**182**(1):534–546.

1148 **Paran I and van der Knaap E**. Genetic and molecular regulation of fruit and plant domestication traits in
1149 tomato and pepper. J Exp Bot. 2007:**58**(14):3841–3852.

1150 **Pease JB, Haak DC, Hahn MW, and Moyle LC**. Phylogenomics Reveals Three Sources of Adaptive
1151 Variation during a Rapid Radiation. PLoS Biol. 2016:**14**(2):e1002379.

1152 **Peng J, Li Z, Wen X, Li W, Shi H, Yang L, Zhu H, and Guo H**. Salt-induced stabilization of EIN3/EIL1
1153 confers salinity tolerance by deterring ROS accumulation in Arabidopsis. PLoS Genet.
1154 2014:**10**(10):e1004664.

1155 **Rao ES, Kadirvel P, Symonds RC, Geethanjali S, Thontadarya RN, and Ebert AW**. Variations in DREB1A
1156 and VP1.1 Genes Show Association with Salt Tolerance Traits in Wild Tomato (Solanum
1157 pimpinellifolium). PLoS One. 2015:**10**(7):e0132535.

1158 **Razali R, Bougouffa S, Morton MJL, Lightfoot DJ, Alam I, Essack M, Arold ST, Kamau AA, Schmöckel**
1159 **SM, Pailles Y, et al.** The genome sequence of the wild tomato Solanum pimpinellifolium provides
1160 insights into salinity tolerance. Front Plant Sci. 2018:**9**:1402.

1161 **Richards LA**. Diagnosis and Improvement of Saline and Alkali Soils (United States Department of
1162 Agriculture).

1163 **Rodriguez M, Scintu A, Posadinu CM, Xu Y, Nguyen CV, Sun H, Bitocchi E, Bellucci E, Papa R, Fei Z, et al.**
1164 GWAS Based on RNA-Seq SNPs and High-Throughput Phenotyping Combined with Climatic Data
1165 Highlights the Reservoir of Valuable Genetic Diversity in Regional Tomato Landraces. Genes .
1166 2020:**11**(11). https://doi.org/10.3390/genes11111387

1167 **Roșca M, Mihalache G, and Stoleru V**. Tomato responses to salinity stress: From morphological traits to
1168 genetic changes. Front Plant Sci. 2023:**14**:1118383.

1169 **Růzicka K, Ljung K, Vanneste S, Podhorská R, Beeckman T, Friml J, and Benková E**. Ethylene regulates
1170 root growth through effects on auxin biosynthesis and transport-dependent auxin distribution.
1171 Plant Cell. 2007:**19**(7):2197–2212.

1172 **Sarfatti M, Abu-Abied M, Katan J, and Zamir D**. RFLP mapping of I1, a new locus in tomato conferring
1173 resistance against Fusarium oxysporum f. sp. lycopersici race 1. Theor Appl Genet. 1991:**82**(1):22–
1174 26.

1175 **Shalata A and Neumann PM**. Exogenous ascorbic acid (vitamin C) increases resistance to salt stress and
1176 reduces lipid peroxidation. J Exp Bot. 2001:**52**(364):2207–2211.

1177 **Shevelev IV and Hübscher U**. The 3’ 5' exonucleases. Nat Rev Mol Cell Biol. 2002:**3**(5):364–376.

1178 **Sievert C**. Interactive Web-Based Data Visualization with R, plotly, and shiny (CRC Press).

1179 **Sousa B, Rodrigues F, Soares C, Martins M, Azenha M, Lino-Neto T, Santos C, Cunha A, and Fidalgo F**.
1180 Impact of Combined Heat and Salt Stresses on Tomato Plants-Insights into Nutrient Uptake and
1181 Redox Homeostasis. Antioxidants (Basel). 2022:**11**(3). https://doi.org/10.3390/antiox11030478

1182 **Steppuhn H and Raney JP**. Emergence, height, and yield of canola and barley grown in saline root zones.
1183 Can J Plant Sci. 2005:**85**(4):815–827.

1184 **Street IH, Aman S, Zubo Y, Ramzan A, Wang X, Shakeel SN, Kieber JJ, and Schaller GE**. Ethylene inhibits
1185 cell proliferation of the Arabidopsis root meristem. Plant Physiol. 2015:**169**(1):338–350.

1186 **Takagi H, Abe A, Yoshida K, Kosugi S, Natsume S, Mitsuoka C, Uemura A, Utsushi H, Tamiru M, Takuno**
1187 **S, et al.** QTL-seq: rapid mapping of quantitative trait loci in rice by whole genome resequencing of
1188 DNA from two bulked populations. Plant J. 2013:**74**(1):174–183.

1189 **Thabet SG, Moursi YS, Sallam A, Karam MA, and Alqudah AM**. Genetic associations uncover candidate
1190 SNP markers and genes associated with salt tolerance during seedling developmental phase in
1191 barley. Environ Exp Bot. 2021:**188**:104499.

1192 **Thole JM, Beisner ER, Liu J, Venkova SV, and Strader LC**. Abscisic acid regulates root elongation through
1193 the activities of auxin and ethylene in Arabidopsis thaliana. G3 (Bethesda). 2014:**4**(7):1259–1274.

1194 **Tripodi P, Soler S, Campanelli G, Díez MJ, Esposito S, Sestili S, Figàs MR, Leteo F, Casanova C, Platani C,**
1195 **et al.** Genome wide association mapping for agronomic, fruit quality, and root architectural traits in
1196 tomato under organic farming conditions. BMC Plant Biol. 2021:**21**(1):481.

1197 **Voiniciuc C**. Modern mannan: a hemicellulose's journey. New Phytol. 2022:**234**(4):1175–1184.

1198 **Wang J, Yu Y, Zhang Z, Quan R, Zhang H, Ma L, Deng XW, and Huang R**. Arabidopsis CSN5B interacts
1199 with VTC1 and modulates ascorbic acid synthesis. Plant Cell. 2013:**25**(2):625–636.

1200 **Wang J and Zhang Z**. GAPIT Version 3: Boosting Power and Accuracy for Genomic Association and
1201 Prediction. Genomics Proteomics Bioinformatics. 2021:**19**(4):629–640.

1202 **Wang X, Gao L, Jiao C, Stravoravdis S, Hosmani PS, Saha S, Zhang J, Mainiero S, Strickler SR, Catala C,**
1203 **et al.** Genome of Solanum pimpinellifolium provides insights into structural variants during tomato
1204 breeding. Nat Commun. 2020a:**11**(1):5817.

1205 **Wang Y, Ji Y, Fu Y, and Guo H**. Ethylene-induced microtubule reorientation is essential for fast inhibition
1206 of root elongation in Arabidopsis. J Integr Plant Biol. 2018:**60**(9):864–877.

1207 **Wang Z, Hong Y, Zhu G, Li Y, Niu Q, Yao J, Hua K, Bai J, Zhu Y, Shi H, et al.** Loss of salt tolerance during
1208 tomato domestication conferred by variation in a Na+ /K+ transporter. EMBO J.
1209 2020b:**39**(10):e103256.

1210 **Website**. https://doi.org/10.1104/pp.111.192088

1211 **Wei T and Simko V**. R package" corrplot": Visualization of a Correlation Matrix (Version 0.84). Retrived
1212 from, https://github com/taiyun/corrplot. 2017.

1213 **Wickham H**. ggplot2: Elegant Graphics for Data Analysis (Springer).

1214 **Wickham H**. reshape2: flexibly reshape data: a reboot of the reshape package. R package version. 2020.

1215 **Wickham H, Averick M, Bryan J, Chang W, McGowan L, François R, Grolemund G, Hayes A, Henry L,**
1216 **Hester J, et al.** Welcome to the tidyverse. J Open Source Softw. 2019:**4**(43):1686.

1217 **Wilke CO**. cowplot: streamlined plot theme and plot annotations for "ggplot2." CRAN Repos. 2016.

1218 **Yang H, Du T, Mao X, Ding R, and Shukla MK**. A comprehensive method of evaluating the impact of
1219 drought and salt stress on tomato growth and fruit quality based on EPIC growth model. Agric
1220 Water Manage. 2019:**213**:116–127.

1221 **Yassin TE**. Inheritance of resistance to leaf curl virus disease in a cross between tomato (Lycopersicon
1222 esculentum Mill.) and currant tomato (L. pimpinellifolium (Jusl.) Mill.). J Agric Sci. 1985:**105**(3):659–
1223 661.

1224 **Ye J, Wang X, Wang W, Yu H, Ai G, Li C, Sun P, Wang X, Li H, Ouyang B, et al.** Genome-wide association
1225 study reveals the genetic architecture of 27 agronomic traits in tomato. Plant Physiol.
1226 2021:**186**(4):2078–2092.

1227 **Zhang R, Li B, Zhao Y, Zhu Y, and Li L**. An essential role for mannan degradation in both cell growth and
1228 secondary cell wall formation. J Exp Bot. 2024:**75**(5):1407–1420.

1229 **Zhang S, Yu H, Wang K, Zheng Z, Liu L, Xu M, Jiao Z, Li R, Liu X, Li J, et al.** Detection of major loci
1230 associated with the variation of 18 important agronomic traits between Solanum pimpinellifolium
1231 and cultivated tomatoes. Plant J. 2018:**95**(2):312–323.

1232 **Zhang Z, Wang J, Zhang R, and Huang R**. The ethylene response factor AtERF98 enhances tolerance to
1233 salt through the transcriptional activation of ascorbic acid synthesis in Arabidopsis. Plant J.
1234 2012:**71**(2):273–287.